Drought Characterization with GPS: Insights into Groundwater and Reservoir Storage in California

Zachary M. Young[1], Hilary R. Martens[1], Zachary H. Hoylman[2], and W. Payton Gardner[1]

[1] Department of Geosciences, University of Montana, Missoula, MT, USA
[2] Montana Climate Office, W.A. Franke College of Forestry and Conservation, University of Montana, Missoula, MT, USA

Corresponding Author:
Zachary M. Young
zachary.young@umt.edu
32 Campus Dr.
Missoula, MT 59812

Key Points:

1. Current drought assessment methods rely primarily on meteorologic drought indices that do not characterize total water storage.
2. The geodetic drought index quantifies hydrologic drought and is especially sensitive to groundwater and reservoir storage.
3. Drought metrics based on geodetic data improve characterization of total water storage, providing unique insight for drought management.

Index Terms:
Geodesy, hydrology, drought, GPS, GNSS, surface-loading

Key Words:
Hydrologic drought index, three-dimensional GPS, GNSS, water management, water resources, atmospheric rivers

ABSTRACT

Drought intensity is commonly characterized using meteorologicly-based metrics that struggle to provide insight into water deficits within deeper hydrologic systems. In contrast, Global Positioning System (GPS) displacements are sensitive to both local and regional hydrologic-storage fluctuations. While a few studies have leveraged this sensitivity to produce geodetic drought indices, hydrologic drought characterization using GPS is not commonly accounted for in drought assessment and management. To motivate this application, we produce a new geodetic drought index (GDI) and quantify its ability to characterize hydrologic drought conditions in key surface and sub-surface hydrologic reservoirs across California. In northern California, the GDI exhibits a strong regional association with reservoir storage at the 1-month time scale (correlation coefficient: 0.83) and groundwater levels at the 3-month time scale (correlation coefficient: 0.87), along with moderate associations with stream discharge at the daily (instantaneous) time scale (correlation coefficient: 0.50). Groundwater in southern California is best characterized with a 12-month GDI (correlation coefficient: 0.77), and reservoir storage is optimized with the 3-month GDI (correlation coefficient: 0.72). Differences between northern and southern California reveal that the GDI is sensitive to unique aquifer and drainage basin characteristics. In addition to capturing long-term hydrologic trends, rapid changes in the GDI initiate during clusters of large atmospheric river events that closely mirror fluctuations in traditional hydrologic and meteorological observations. We show that GPS-based hydrologic drought indices provide a significant opportunity to improve drought assessment, in California and beyond, by improving our understanding of the hydrologic cycle.

PLAIN LANGUAGE SUMMARY

Although quantifying the total volume of water loss is of critical importance during periods of drought, drought intensity is often characterized using meteorologic observations, such as precipitation, rather than using more holistic hydrologic observations, such as reservoir levels and groundwater. While precipitation is a good measure of the amount of water entering a region, precipitation models struggle to determine the amount of water retained in a watershed or the amount lost due to runoff and evapotranspiration. An important distinction when determining appropriate approaches for drought management. We address this need by producing a hydrologically based drought index that captures changes in both surface and subsurface hydrologic reservoirs using surface-loading geodesy, which quantifies changes in water volume based on how the shape of the Earth changes under the weight of

the water. In this study, we use three-dimensional Global Positioning System data to develop a geodetic drought index (GDI). Comparison with independent hydrologic observations indicates strong regional and temporal correlations with reservoir storage, groundwater fluctuations, and stream discharge observations, suggesting the GDI can effectively characterize variations in total hydrologic storage. The GDI provides an opportunity to improve hydrologic models for drought management and to advance our understanding of the water cycle.

1 INTRODUCTION

Groundwater is a critical resource for sustaining natural and human ecosystems, and sufficient reserves are necessary to endure periods of sustained drought (Famiglietti, 2014; Rodell et al., 2018). This reality has become particularly evident in recent years following the intense droughts within California (Argus et al., 2017; He et al., 2017; Liu et al., 2022; Prein et al., 2016; Williams et al., 2022; Xiao et al., 2017). The persistent droughts in this region have threatened drinking water supplies and influenced agricultural production, resulting in increased local and regional economic burdens (Medellín-Azuara et al., 2022; Mishra & Singh, 2010). This has highlighted the importance of improving water resource management techniques and advancing our understanding of the current state of terrestrial water storage (TWS) (Wilhite et al., 2007). While many metrics exist to quantify the intensity of drought (e.g. the U.S. Drought Monitor [USDM; Svoboda et al., (2002)], the Palmer Drought Severity Index [PDSI; Palmer (1965)], and the Standardized Precipitation Evapotranspiration Index [SPEI; Vicente-Serrano et al., (2010)], etc.), the drought indices that are primarily used to influence drought assessment and management decisions are driven by meteorological data and thus are particularly indicative of meteorological drought conditions. Hence, these metrics provide useful insight into meteorologic moisture input over time, but do not characterize TWS retention for a given region.

To understand how anomalies in TWS vary, and thus to assess drought conditions associated with the entire hydrological system, a hydrologically based drought index with input data sensitive to all surface and subsurface moisture is necessary. Toward this goal, hydrologic drought indices have been developed using Gravity Recovery and Climate Experiment (GRACE) observations [i.e., the GRACE Data Assimilation System (Houborg et al., 2012; Li et al., 2019), the GRACE Drought Severity Index (Zhao et al., 2017), and the GRACE Groundwater Drought Index (Thomas et al., 2017)]. While an intriguing application of geodetic observations, these indices are most applicable to large regional/continental scale drought characterization given the spatio-temporal resolution of the original input GRACE data (i.e., monthly at ~300 km).

Alternatively, Chew & Small (2014) introduced a successful small-scale example of a novel approach to characterizing TWS anomalies at both local and regional scales, with high temporal resolution. Here, the authors leverage the relationship between the elastic response of the solid Earth and vertical Global Positioning System (GPS) displacements (White et al., 2022), to produce a GPS based drought metric. The fundamental conceptional model driving this metric, and hydrogeodesy in

general, is as follows: during dry periods, water leaves the system and unloads the surface of the Earth causing the ground elevation to rise. Conversely, when water enters the system, the surface is loaded, and the Earth's surface subsides. In addition, the ground moves horizontally towards a source of loading and away from a region of unloading. GPS data are particularly sensitive to these displacements and have been used to both localize and quantify hydrologic load variation across a wide range of spatio-temporal scales (Amos et al., 2014; Argus et al., 2014, 2017; Borsa et al., 2014; Fu et al., 2013, 2015; Knappe et al., 2019; Larochelle et al., 2022; Overacker et al., 2022; White et al., 2022; Young et al., 2021). The motions observed by GPS represent the combined response to the entire water column of both local/regional spatial trends and short-/long-term temporal trends. Thus, the geodetic observations of surface loading provide an opportunity to isolate signals associated with specific hydrologic changes that exhibit trends at different temporal scales [e.g., reservoir storage varies at shorter drainage-basin time scales than groundwater, which varies based on a combination of aquifer characteristics (Skøien et al., 2003) and anthropogenic effects (Laveti et al., 2021; Wu et al., 2020)].

Since Chew & Small (2014), several studies have built upon their methods to assess drought characteristics by developing Geodetic Drought Indices (GDIs) [also termed GNSS-based Drought Indices, referring generally to any Global Navigation Satellite System (GNSS)] driven by vertical GPS displacements (Ferreira et al., 2018; Jiang et al., 2022b), or hydrologic loading estimates calculated from vertical GPS displacements (Jiang et al., 2022a; Tang et al., 2023). Although these studies advance the methods of Chew & Small (2014) with differing approaches over different spatio-temporal scales (see Table 1), each successfully characterize hydrologic drought within their respective regions using combinations of GRACE, hydrologic models, and meteorologic drought indices as validation. Lending support to the strength of the fundamental core of the methodology to assess hydrologic drought variation through the use of GPS displacement time series.

While useful, these studies do not directly compare geodetic observations with more holistic hydrologic observations such as groundwater levels or reservoir storage observations. This distinction is critical to evaluate the sensitivity of geodetic observations to different hydrologic reservoirs and assessing the strength of hydrologic drought characterization, particularly from the standpoint of active drought management where GDIs have yet to gain traction.

By deriving hydrologic loading estimates from the vertical GPS displacement fields, Jiang et al. (2022a) provide a more robust characterization of hydrologic drought by leveraging the response of the entire GPS network (White et al., 2022), as opposed to solely relying on individual station

displacements, from which it is difficult to disentangle local and regional signals. For example, the motion of a station may be influenced by an increase in discharge at a nearby river, as well as by the loading of a lake in a neighboring valley. In combination with nearby stations, the magnitude and distribution of these loads can be estimated. When inverting for loads using the entire GPS network, we identify the spatial distribution of TWS that best explains the combined regional response of all stations in the network to hydrologic loading across both local and regional scales. Tang et al. (2023) further advance the methodology by deriving their index comparably to the SPEI, thus producing a multi-scale hydrologic drought index which leverages the sensitivity of the GPS displacements to the different temporal scales of hydrologic variation. In addition, this allows comparability of regional trends regardless of spatial gradients in the magnitude of TWS estimates, facilitating comparison of drought characteristics across various climates where TWS magnitude can vary substantially. Thus, modeling the GDI after the well-established SPEI represents a significant advancement, which we intend to expand upon in this study.

Both Jiang et al. (2022a) and Tang et al. (2023) adopted a Slepian Basis Function approach to calculate hydrologic loading estimates rather than the more traditional spherical harmonics method. This choice is driven by the need to address the sparse spatial resolution of the GPS network in Brazil, and the resolution of the functions approximately matched the spatial resolution of GRACE (Jiang et al. 2022). For regions where the GPS network is relatively dense, such as California, higher spatial resolutions are required in the modeling to recover localized hydrologic variation.

In this study, our goal is to further advance the methodologies of Tang et al. (2023) to produce a new multi-scale geodetic drought index forced by hydrologic loading estimates. The loading estimates are derived using the LoadDef software suite (Martens et al., 2019). For our analysis, we experiment with including horizontal GPS components to assess whether we obtain improved load localization using three-dimensional displacements (rather than vertical only), an aspect which has not been explored in previous GDI studies. Following Tang et al. (2023), we derive our index comparably to the SPEI (Vicente-Serrano et al., 2010); however, we expand the input distribution such that the GDI is insensitive to the chosen characterization distribution [i.e., log-logistic, as applied by Vicente-Serrano et al. (2010), or the normal distribution, applied by Tang et al. (2023)]. We apply the new GDI to a case study within California, and directly assess the capabilities of the GDI by comparing different time scales of the GDI with daily observations of groundwater levels, reservoir storage, stream discharge, and soil moisture anomalies; a novel approach to assess the utility of the GDI to capture different

components of hydrologic drought. This approach provides an opportunity to better understand TWS fluctuations within specific hydrologic reservoirs and drainage basins, including with respect to groundwater and reservoir storage. Furthermore, the results showcase the tremendous opportunities for GPS-based GDIs to improve hydrologic models and drought management at local and regional scales.

166 **Table 1:** Comparison of the methods presented in this study with prior developments and investigations of geodetically
167 informed drought indices. Validation model acronyms: GRACE:Gravity Recovery and Climate Experiment (including
168 indexed versions), NLDAS: North American Land Data Assimilation System, scPDSI: Self-calibrating Palmer Drought
169 Severity Index, STI: Standardized Temperature Index, SPI; Standardized Precipitation Index, SPEI: Standardized
170 Precipitation Evapotranspiration Index, and the USDM: United States Drought Monitor.
171

Study	**Region**	**GPS Stations**	**GPS Components**	**GPS Application**	**Load Calculation Method**	**Estimation Strategy**
Chew & Small (2014)	Midwestern U.S.	15	Vertical	Displacement	~	Displacement anomaly time series stacking
Ferreira et al., (2018)	Brazil	39	Vertical	Displacement	~	Displacement anomaly time series stacking
Jiang et al, (2022a)	Brazil	104	Vertical	Hydrologic Loading	Slepian Basis Functions	Least squares with second order Tikhonov regularization
Jiang et al., (2022b)	Continental U.S.	1900	Vertical	Imaged Displacement	~	Spatial Filtering
Tang et al., (2023)	Brazil	104	Vertical	Hydrologic Loading	Slepian Basis Functions	Least squares
This Study	*Southwestern US/California*	*1158*	*3-Dimensional*	*Hydrologic Loading*	*LoadDef*	*Iteratively Reweighted Least Squares with zeroth and second order Tikhonov regularization*
Study	**Time Scale**	**Spatial Resolution**	**Temporal resolution**	**Initial GPS Data Filtering**	**Earth Model**	**Model Validation**
Chew & Small (2014)	Uni-scale	GPS Network	Daily	GPS Low pass	~	GRACE, Precipitation, USDM
Ferreira et al., (2018)	Uni-scale	GPS Network	Monthly	GPS Monthly normal removed	~	GRACE

Jiang et al, (2022a)	Uni-scale	Not provided?	Monthly	GPS 7 day median window	Not provided	GRACE
Jiang et al., (2022b)	Uni-scale	0.25°	Monthly	GPS PCA	~	GRACE, NLDAS, USDM, scPDSI
Tang et al., (2023)	Multi-scale SPEI (normal distribution)	1°	Daily	None	Average Earth Density	GRACE, STI, SPI, SPEI
This Study	*Multi-scale SPEI (three-parameter log-logistic distribution)*	*0.25°*	*Daily*	*None*	*PREM*	*Groundwater wells, reservoir storage, reservoir height, stream discharge, soil moisture, SPEI, USDM*

2 METHODS

2.1 HYDROLOGIC LOAD ESTIMATION

To relate observed GPS displacements to hydrologic loading we use the LoadDef software suite (Martens et al., 2019), which uses spherical harmonics to evaluate loading displacements on a self-gravitating sphere. Here we use the Preliminary Reference Earth Model (PREM) (Dziewonski & Anderson, 1981) to define the material properties of Earth's interior. This approach accounts for finer-scale and more realistic features compared to Tang et al. (2023), where the model relied solely on the average Earth density, rather than a stratified structure (Table 1). The bounds of the model are constrained to a latitude range of 30º – 44º N and a longitude range of -125º – -104º E (Figure S1). We opt for the wider longitude range such that loading exterior to our primary study area of California is well accounted for. North of 44º, the effects of slow slip events along the Cascadia subduction zone become more prevalent so we do not extend the study area further northward.

To address far-field loading outside of the model region, we forward model surface displacements based on the GRACE mascon solutions within three degrees of the edge of our expanded study area (Wiese et al., 2023), and remove them from our time series. Loading effects beyond three degrees are negligible for the purposes of our study. Changes in water volume and their spatial distribution are calculated on a regular grid at 0.25º resolution and the forward-model calculation is evaluated at 0.01º resolution using a common geographic mesh. To avoid sharp changes in water

storage across neighboring grid cells, the solution is regularized with a combination of zeroth and second-order Tikhonov regularization [Aster & Thurber (2013); Equation 1].

Equation 1: $$f(m) = ||Gm - d||_2 + \lambda_1||Im||_2 + \lambda_2||Lm||_2$$

Here *G* is the design matrix, *m* is the model vector, *d* is the GPS observation data vector, *I* is the identity matrix, *L* is the 2-D discrete Laplacian regularization matrix, and λ_1 and λ_2 are hyperparameters used to optimize the solution.

Loading studies often filter the input GPS time series to weekly or monthly time scales, and/or adopt strict data-cleaning regimens, to account for scatter in the GPS data (Argus et al., 2017; Chew & Small, 2014; Fu et al., 2013, 2015; Jiang et al., 2022; White et al., 2022). For our study, we do not want to inadvertently introduce bias into the solution by smoothing the input time series or applying data cuts based on uncertainty thresholds as this can omit important signals during rapid load variation [e.g. following atmospheric river (AR) events (Rutz & Steenburgh, 2012) and flash droughts (Ahmad et al., 2022; Otkin et al., 2018)]. Thus, we adopt the iteratively reweighted least squares (IRLS) approach within the load inversion, which mitigates the influence of outliers by reweighting the solution for each epoch based on the model residuals (Aster & Thurber, 2013). The solution is allowed to iterate until the model and residual vectors converge to a tolerance value of $\tau < 0.005$, following Equation 2. For the first iteration, we perform a standard weighted least-squares inversion. To prevent over-fitting and ensure convergence, residuals are fixed to a value of 0.01 mm when they fall below this cutoff.

Equation 2: $$\frac{||m^{k+1} - m^k||_2}{1 + ||m^{k+1}||_2} < \tau$$

The hyperparameters λ_1 and λ_2 are optimized for the solution that best minimizes the norm of the residuals ($||d\text{-}Gm||_2$), the solution semi-norm ($||Lm||_2$), and the zeroth order norm ($||Im||_2$) concurrently. These are identified from a suite of 113 days, spread evenly across the study period, for which λ_1 and λ_2 are tested over a range of values. The values $\lambda_1 = \lambda_2 = 1.5$ most frequently optimize the solution and are used to produce the full suite of load solutions.

2.2 GEODETIC DROUGHT INDEX CALCULATION

We develop the GDI following Vicente-Serrano et al. (2010) and Tang et al. (2023), such that the GDI mimics the derivation of the SPEI, and utilize the log-logistic distribution (further details below). While we apply hydrologic load estimates derived from GPS displacements as the input for this GDI (Figure 1a-d), we note that alternate geodetic drought indices could be derived using other types of geodetic observations, such as InSAR, gravity, strain, or a combination thereof. Therefore, the GDI is a generalizable drought index framework.

A key benefit of the SPEI is that it is a multi-scale index, allowing the identification of droughts which occur across different time scales. For example, flash droughts (Otkin et al., 2018), which may develop over the period of a few weeks, and persistent droughts (>18 months), may not be observed or fully quantified in a uni-scale drought index framework. However, by adopting a multi-scale approach these signals can be better identified (Vicente-Serrano et al., 2010). Similarly, in the case of this GPS-based GDI, hydrologic drought signals are expected to develop at time scales that are both characteristic to the drought, as well as the source of the load variation (i.e., groundwater versus surface water and their respective drainage basin/aquifer characteristics). Thus, to test a range of time scales, the TWS time series are summarized with a retrospective rolling average window of D (daily with no averaging), 1, 3, 6, 12, 18, 24, 36, and 48-months width (where one month equals 30.44 days).

From these time-scale averaged time series, representative compilation window load distributions are identified for each epoch. The compilation window distributions include all dates that range ±15 days from the epoch in question per year. This allows a characterization of the estimated loads for each day relative to all past/future loads near that day, in order to bolster the sample size and provide more robust parametric estimates [similar to Ford et al., (2016)]; this is a key difference between our GDI derivation and that presented by Tang et al. (2023). Figure 1d illustrates the representative distribution for 01 December of each year at the grid cell co-located with GPS station P349 for the daily TWS solution. Here all epochs between between 16 November and 16 December of each year (red dots), are compiled to form the distribution presented in Figure 1e.

This approach allows inter-annual variability in the phase and amplitude of the signal to be retained (which is largely driven by variation in the hydrologic cycle), while removing the primary annual and semi-annual signals. Solutions converge for compilation windows >±5 days, and show a minor increase in scatter of the GDI time series for windows of ±3-4 days (below which instability becomes more prevalent). To ensure robust characterization of drought characteristics, we opt for an extended ±15-day compilation window. While Tang et al. (2023) found the log-logistic distribution to

be unstable and opted for a normal distribution, we find that, by using the extended compiled distribution, the solutions are stable with negligible differences compared to the use of a normal distribution. Thus, to remain aligned with the SPEI solution, we retain the three-parameter log-logistic distribution to characterize the anomalies. Probability weighted moments for the log-logistic distribution are calculated following Singh et al., (1993) and Vicente-Serrano et al., (2010). The individual moments are calculated following Equation 3.

Equation 3: $$w_s = \frac{1}{N}\sum_{i=1}^{N} x_{s_i}(1 - F_i); s = 0, 1, 2$$

These are then used to calculate the L-moments for shape (α), scale (β), and location (γ) of the three-parameter log-logistic distribution (Equations 4 – 6).

Equation 4: $$\beta = \frac{2w_1 - w_0}{6w_1 - w_0 - 6w_2}$$

Equation 5: $$\alpha = \frac{\beta(w_0 - 2w_1}{\Gamma(1+\frac{1}{\beta})\Gamma(1-\frac{1}{\beta})}$$

Equation 6: $$\gamma = w_0 - \alpha\Gamma(1 + \tfrac{1}{\beta})\Gamma(1 - \tfrac{1}{\beta})$$

where $\Gamma(z)$ is the gamma function of z.

The probability density function (PDF) and the cumulative distribution function (CDF) are then calculated following Equations 7 and 8, respectively.

Equation 7: $$f(x) = \frac{\beta}{\alpha}(\frac{x-\gamma}{\alpha})^{\beta-1}[1 + (\frac{x-\gamma}{\alpha})]^{-2}$$

Equation 8: $$F(x) = [1 + (\frac{\alpha}{x-\gamma})^{\beta}]^{-1}$$

The inverse Gaussian function is used to transform the CDF from estimates of the parametric sample quantiles to standard normal index values that represent the magnitude of the standardized anomaly. Here, positive/negative values represent greater/lower than normal hydrologic storage. Thus,

an index value of -1 indicates that the estimated load is approximately one standard deviation dryer than the expected average load on that epoch. Drought intensity is classified following Table 2 (Svoboda et al., 2002). Figure 1e provides an example of the fit of the log-logistic distribution to the compiled distribution of loads for 01 December of each year (Figure 1d). The GDI for 01 December 2013, is -0.24, which is within normal water-storage levels. By 01 December 2015, however, the GDI reduces to -1.50, indicating severe hydrologic drought. Following California's significant precipitation years of 2016 and 2017, the GDI increases to 1.97 on 01 December 2017, indicating storage has recharged to extremely high hydrologic storage levels at this location.

Table 2: U.S. Drought Monitor SPEI categories of Svoboda et al. (2002), and our expanded GDI drought categories.

Category	USDM SPEI	GDI	Anomaly
W4	~	Exceptionally High Hydrologic Storage	>2
W3	~	Extremely High Hydrologic Storage	1.6 to 2
W2	~	Especially High Hydrologic Storage	1.3 to 1.59
W1	~	Moderately High Hydrologic Storage	0.8 to 1.29
W0	~	Abnormally Wet	0.5 to 0.79
None	Normal	Normal	-0.49 to 0.49
D0	Abnormally Dry	Abnormally Dry	-0.5 to -0.79
D1	Moderate Meteorologic Drought	Moderate Hydrologic Drought	-0.8 to -1.29
D2	Severe Meteorologic Drought	Severe Hydrologic Drought	-1.3 to -1.59
D3	Extreme Meteorologic Drought	Extreme Hydrologic Drought	-1.6 to -2
D4	Exceptional Meteorologic Drought	Exceptional Hydrologic Drought	< -2

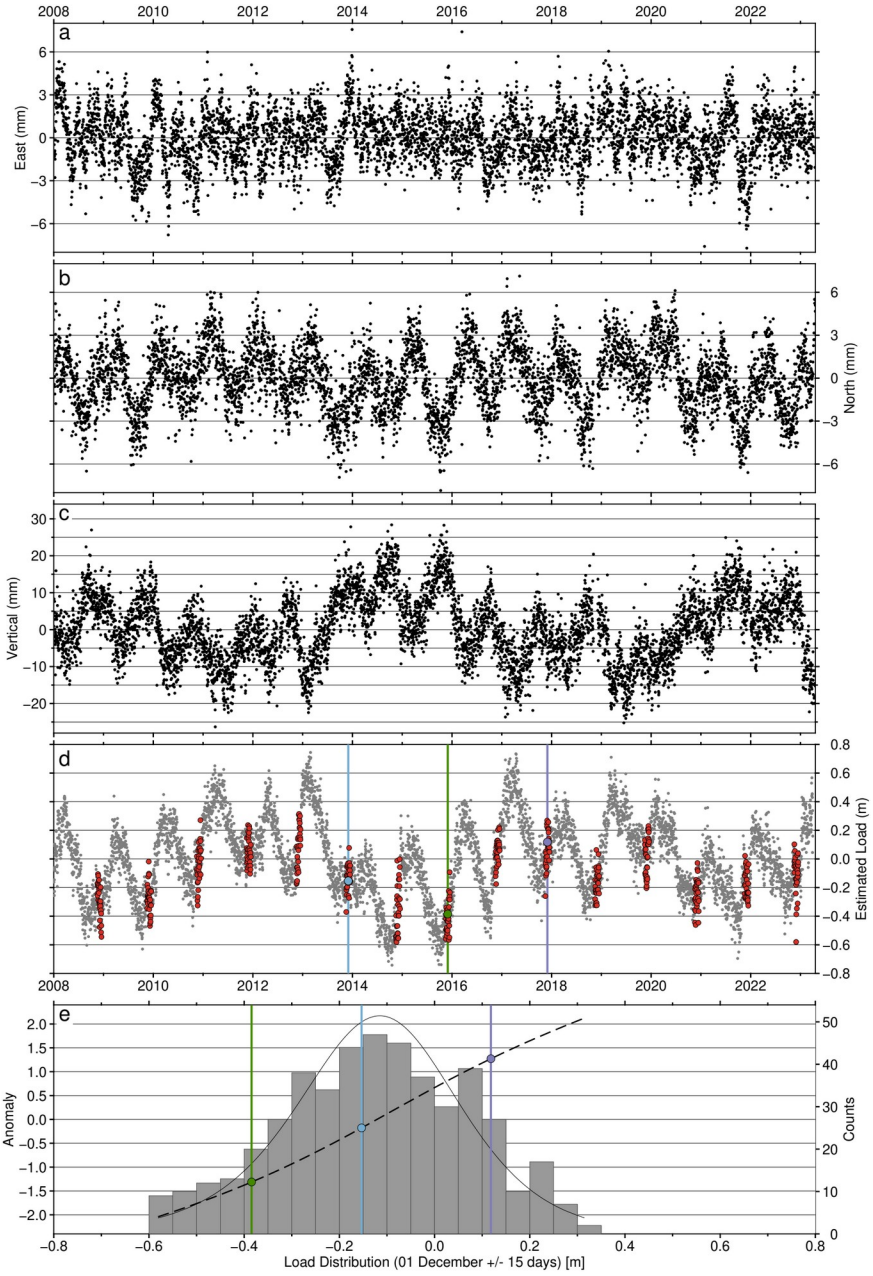

Figure 1: Example GDI calculation. Corrected and detrended (a) east, (b) north, and (c) vertical displacements for GPS station P349, which is located near the southern shoreline of Lake Shasta. Note the difference in scales between the horizontal and vertical components. (d) Daily load estimates for the grid cell co-located with GPS station P349 (grey dots). The blue dot and vertical line identify 01 December 2013, while the green and purple dots/vertical lines identify 01 December 2015 and 2017, respectively. The red dots highlight the epochs ± 15 days from these dates, which are used to compile the distribution of terrestrial water storage (TWS) estimates for characterizing the GDI on these dates. (e) Histogram of TWS estimates for 01 December ± 15 days overlain with

the shape of the log-logistic PDF (black line) for these data. The dashed black line shows the GDI for this distribution and the colored dots/vertical lines reflect the epochs noted in panel d.

3 DATA

3.1 GPS OBSERVATIONS

We use GPS data and a catalog of time series steps from the Nevada Geodetic Laboratory (NGL; Blewitt et al., 2018). Time series are produced using the GipsyX software in the IGS14 reference frame (Altamimi et al., 2016; Bertiger et al., 2020). Initially, 2509 GPS stations are available within our study area. We discard stations with less than eight years of data between 01 January 2008 and 31 March 2023. This threshold is chosen to prevent stations with short data records, which may not have enough observations to distinguish drier/wetter periods, from biasing the solution. Stations that exhibit poro-elastic deformation or transient motions associated with volcanic centers are omitted (Argus et al., 2014; Kang & Knight, 2023; White et al., 2022), leaving 1160 stations for our analysis (Figures 2 & S1). The minimum number of concurrent observations is 795 stations on 02 February 2008, and the maximum of 1131 stations occurs on 09 April 2015, with an average of 1027 stations across the study period.

The steps catalog for each station represents a combination of both mechanical/equipment changes and possible earthquake-related offsets. Many of these steps do not impart a noticeable offset, and some stations have offsets that are not indicated in the list; thus, we manually inspect the time series for each station to ensure steps are appropriately accounted for, and the catalog is modified accordingly on a component-by-component basis. Periods of problem data due to known sources [e.g., early postseismic deformation (< 1 year) and multipath] and unknown sources (e.g., spurious periods of elevated scatter) are manually identified and removed. Long-term postseismic deformation significantly affects the horizontal components of the GPS stations in this region, and we correct the time series using the postseismic model of Young et al. (2023). Each station is then corrected for non-tidal atmospheric and oceanic pressure loading using the GFZ-Potsdam gridded solutions (Dill & Dobslaw, 2013). Offsets from the updated step catalog are then calculated and corrected, after which the linear velocity trend is removed. Annual and semi-annual signals are retained in the time series and accounted for during the GDI calculation.

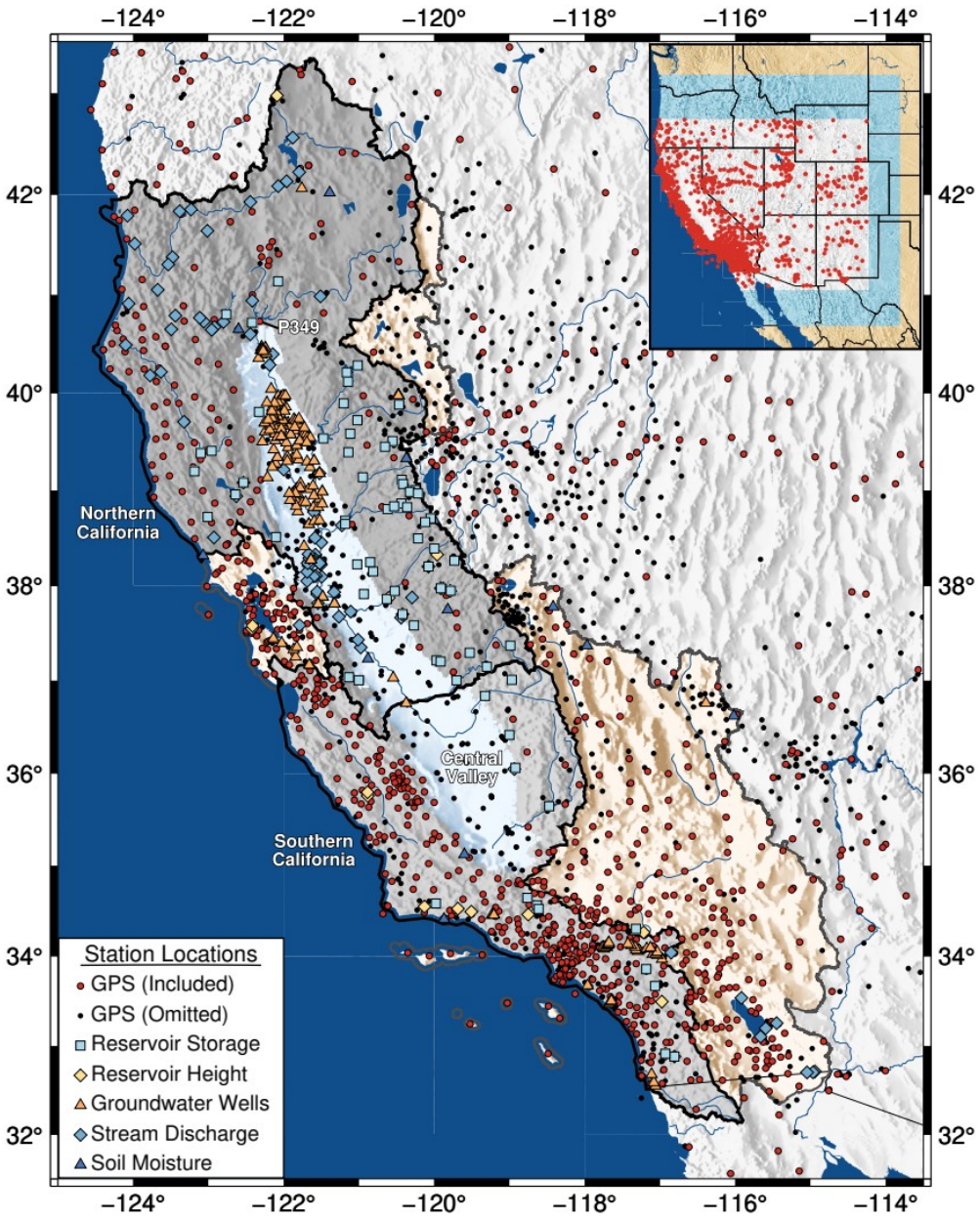

Figure 2: Regional map showing the distribution of GPS and hydrologic stations in and around California. The full study area is shown in the inset and Figure S1. Accepted GPS stations are shown as red circles while those omitted are presented as black dots. Reservoir storage locations, with volume data, are shown as light blue squares and lake/reservoir water surface height gauges, with only elevation data, are yellow diamonds. Groundwater wells are presented as orange triangles. Stream discharge gauges are shown as blue diamonds and soil moisture stations are identified as dark blue triangles. The Northern and Southern California sub-region boundaries (thick black lines with grey shading) are a combination of level 4 hydrologic unit code regions (Jones et al., 2022). Remaining California sub-region boundaries are shown with thick grey

lines and tan shading. Thin blue lines show river locations. California's Central Valley is highlighted with light blue shading. The location of GPS station P349, near Lake Shasta in northern California, is indicated with a black line from its label. Inset shows an expanded view of the full study area. The load calculation region is shown with grey shading and overlain with the included GPS station locations as grey dots. The region used to calculate far-field loading with GRACE is shaded in blue. No data is used from the tan region.

3.2 HYDROLOGIC OBSERVATIONS

Data for reservoir storage, reservoir/lake surface height, groundwater well height (level), and stream discharge are obtained from the National Water Information System (NWIS) (U.S. Geological Survey, 2016). Additional reservoir storage data is obtained from CDEC (California Data Exchange Center, 2023), and continuous and periodic groundwater well data from the California Department of Water Resources Water Data Library and the California Natural Resources Agency (California Natural Resources Agency, 2023a, 2023b; Water Data Library, 2023a, 2023b). For each of these data sets, station time series are inspected, and problem stations are removed (i.e., those that show clear indications of sensor or monumentation issues). To be considered, stations must meet the same temporal requirements as the GPS data. Hydrologic data outside of California is sparse (Figure S1), thus we limit our analysis to those hydrologic stations located within California (Figure 2).

Reservoir storage stations are limited to those that retain median storage volumes greater than 0.02 km^3. For reservoirs that experience periods of no water storage, these periods are omitted. Finally, many reservoirs are actively managed and therefore exhibit limited volume variation (i.e., their annual signal is nearly constant in both phase and amplitude); thus, they do not reflect regional hydrologic variation trends and are omitted. Following these constraints, we consider 72 reservoirs in our analysis. The NWIS additionally provides surface height data for a combination of 20 reservoirs and lakes within the region. Although these data do not account for the complexity of the local geography, globally many lakes and reservoirs do not contain adequate data to constrain volume estimates. Thus, it is useful to compare the GDI to both reservoir storage and reservoir/lake height observations to understand and interpret the GDI at these locations.

We restrict the groundwater well data to stations identified by the NWIS to be within either unconfined or semi-confined aquifers. The CNRA and WDL groundwater data do not indicate aquifer type, but they are located near NWIS groundwater stations and within the Central Valley, therefore, we include them. Groundwater well data that exhibit an active pumping signal or do not contain annual

signals in their time series (Houborg et al., 2012), are removed, leaving 193 groundwater well stations within California.

Stream discharge time series are generally well behaved (i.e., they exhibit few periods of spurious outliers or steps in their time series); however, many stations are placed on minor streams or exhibit infrequent flow. To ensure stations are most reflective of drainage-basin dynamics throughout the year, stations are limited to those whose median discharge across the study period is greater than 5 $m^3 s^{-1}$, which leaves 70 gauges for our analysis. Soil moisture data was accessed from publicly available data sources including the Soil Climate Analysis Network (SCAN), Snow Telemetry (SNOTEL) and the U.S. Climate Reference Network (USCRN). Of these data, eleven soil moisture stations are available within California.

To directly compare and quantify the relationship between the GDI and hydrologic observations, each hydrologic data set is passed through the same processing workflow as the GPS data, except that only the daily (rather than time-integrated) solutions calculated and a gamma distribution was used for the soil moisture data (see Supplemental Text S1 for more details). This facilitates the identification of optimal time frames for the GDI that best represent specific hydrologic processes.

3.3 ATMOSPHERIC RIVERS

Atmospheric Rivers (ARs) are concentrated bands of water vapor that produce significant rainfall over a series of days, rapidly altering the mass distribution of the impacted region (Rutz et al., 2014; Rutz & Steenburgh, 2012). These events are a key driver of hydrologic storage fluctuation; thus, we expect to observe an association between drought severity and the frequency of AR activity, reflected in both the hydrologic observations as well as in the GDI. To explore this, we obtain a gridded AR catalog from the Center for Western Weather and Water Extremes (Rutz et al., 2014, 2019). For both the northern and southern California regions (Figure 2), we identify the peak integrated water vapor transport on each epoch to produce subcatalogs of peak AR activity, which we then compare with hydrologic anomalies and the GDI. The largest influence on drought severity is expected to occur during the most significant AR events; thus, we limit the subcatalogs to the highest intensity ARs (3+).

4 APPLICATION OF THE GPS-BASED GDI TO CALIFORNIA

405 4.1 CHARACTERIZATION OF LAKE SHASTA STORAGE

406 Lake Shasta is the largest man-made reservoir in California and its storage exhibits strong
407 annual signals (Figure 3a). GPS station P349 lies only 2 km south of the reservoir and exhibits a strong
408 annual signal in its vertical component (Figure 1c). The correlation coefficient between the vertical
409 displacements and the water storage in the reservoir is -0.67, highlighting the inverse relationship
410 between hydrologic loading and surface displacement. Considering the strength of the correlation, the
411 GDI is expected to strongly reflect load variation within the reservoir. Figure 3b shows a comparison
412 between the 1-month GDI (i.e., the TWS time series is smoothed with a 1-month retrospective rolling
413 average window prior to GDI calculation) for the grid cell co-located with P349 and the daily reservoir
414 storage index for Lake Shasta. The correlation coefficient between these two indices is strong, at 0.85,
415 indicating the GDI is representative of the load variation across the entire study period within the
416 reservoir and performs better than a direct comparison between the GPS displacements and the
417 reservoir storage. When comparing the reservoir storage to the daily indexed GDI, the correlation
418 coefficient is 0.77. This shows that both the use of the load solution, due to leveraging the entire GPS
419 network, and smoothing to the 1 month time scale, improve the solution. At the longer time scales of
420 3-, 6- and 12-months the correlation coefficients decline to 0.83, 0.77, and 0.64, revealing the 1-month
421 GDI solution as the optimal time scale.

422 On shorter time scales, rapid increases in reservoir volume are driven by precipitation, with the
423 largest changes occurring during AR events (Rutz et al., 2014). Sharp increases to wetter (positive)
424 GDI anomalies align well with the occurrence of category 3+ AR events within California (gray
425 vertical lines). This indicates the GDI is sensitive not only to long-term trends of loading at and near
426 Lake Shasta, but also to reservoir volume variations driven by strong precipitation events. This is
427 particularly evident in the Decembers of 2012 and 2014 – 2016, during which clusters of AR events are
428 directly followed by sharp GDI increases toward wetter conditions.

429

430

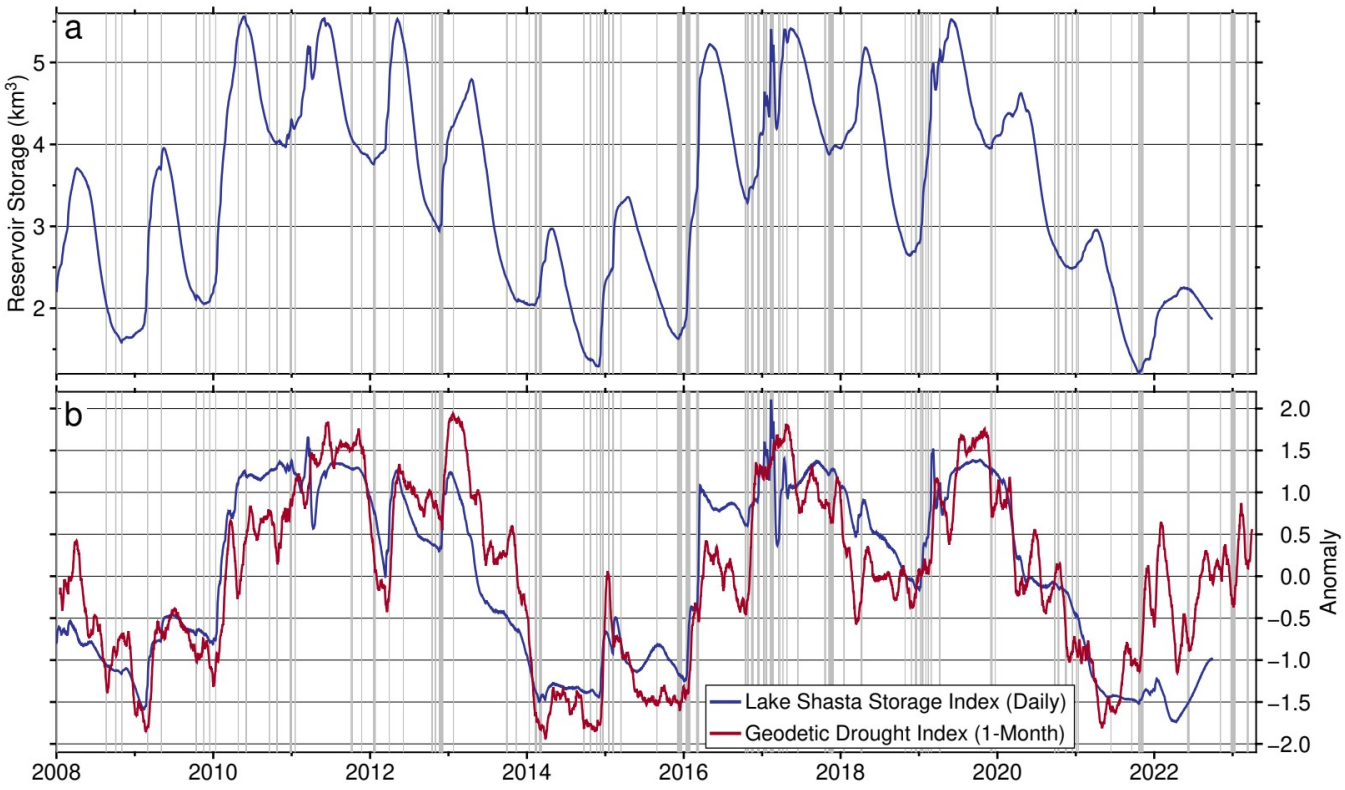

Figure 3: Comparison of the GDI with Lake Shasta reservoir storage. (a) Observed daily reservoir storage values for Lake Shasta. (b) Comparison of the 1-month GDI with the daily reservoir storage index for Lake Shasta (correlation coefficient: 0.85). Background vertical grey bars represent category 3+ atmospheric river (AR) events that impacted northern California.

4.2 REGIONAL CORRELATIONS

To understand how different time scales of the GDI relate to variation within specific hydrologic reservoirs, and to gain insight into their respective regional dynamics for use with future drought management, we consider three cases. In the first, a “co-located” case, we compare the unique GDI grid cells that contain hydrologic stations with each daily indexed hydrologic anomaly data set (i.e., only the grid cells containing groundwater stations are compared with the groundwater anomalies, Figure 2). For each data set, the time series are stacked and the median anomaly is calculated for each epoch and compiled to produce a median anomaly time series. The correlation coefficient is then calculated between the different time scales of the GDI and the hydrologic data. For both the “Northern California” and “Southern California” cases, we limit both the GDI and the hydrologic observations to those data within their respective watershed boundaries (Figure 2). Results, presented in Figure 4 and

Table 3, are limited to data sets that contain at least five concurrent observations for most of the time period.

In the local case, optimal GDI time scales for groundwater wells, reservoir storage, reservoir height, and stream discharge are found at the 3-, 1-, 3-, and 1-month time scales, respectively, with correlation coefficients of 0.88, 0.81, 0.69, and 0.47 (Figure 4a). Soil moisture shows no clear relationship with any GDI time scale. For the groundwater wells, reservoirs, and stream discharge data sets, correlation coefficients decline rapidly away from the optimal GDI time scale. When the hydrologic observations are separated into the northern and southern regions of California, the groundwater wells exhibit significantly different optimal time scales. In northern California, the groundwater wells (which are primarily located within the northern Central Valley, Figure 2) exhibit the strongest correlations at the 1- and 3- month GDI time scales (Figure 4b). Conversely, in southern California, the groundwater wells (which are located within California Coastal Basin aquifers) exhibit the strongest correlation of 0.77 at the 12-month GDI time scale (Figure 4c). Correlation coefficients for both reservoir storage and reservoir height are higher in northern California and peak at the 1-month GDI time scale, at 0.83 and 0.63 respectively. In southern California, reservoir storage and reservoir height correlations with the GDI peak later (at the 3-month time scale) with correlation coefficients of 0.72 and 0.56, respectively. We estimate that the two-sigma uncertainty in each of the correlation coefficients is approximately ± 0.03, based on a distribution of 10,000,000 correlation coefficients calculated between the hydrologic observations and randomized GDI time series.

Data limitations prevent comparison of stream discharge and soil moisture between the three regional case studies, but we note that stream discharge improves slightly at the daily GDI time scale in northern California compared to the co-located case. The case-study results reveal two clear findings. First, the GDI strongly characterizes hydrologic observations across California. Second, the GDI reflects unique aquifer and drainage basin characteristics between the northern and southern California regions.

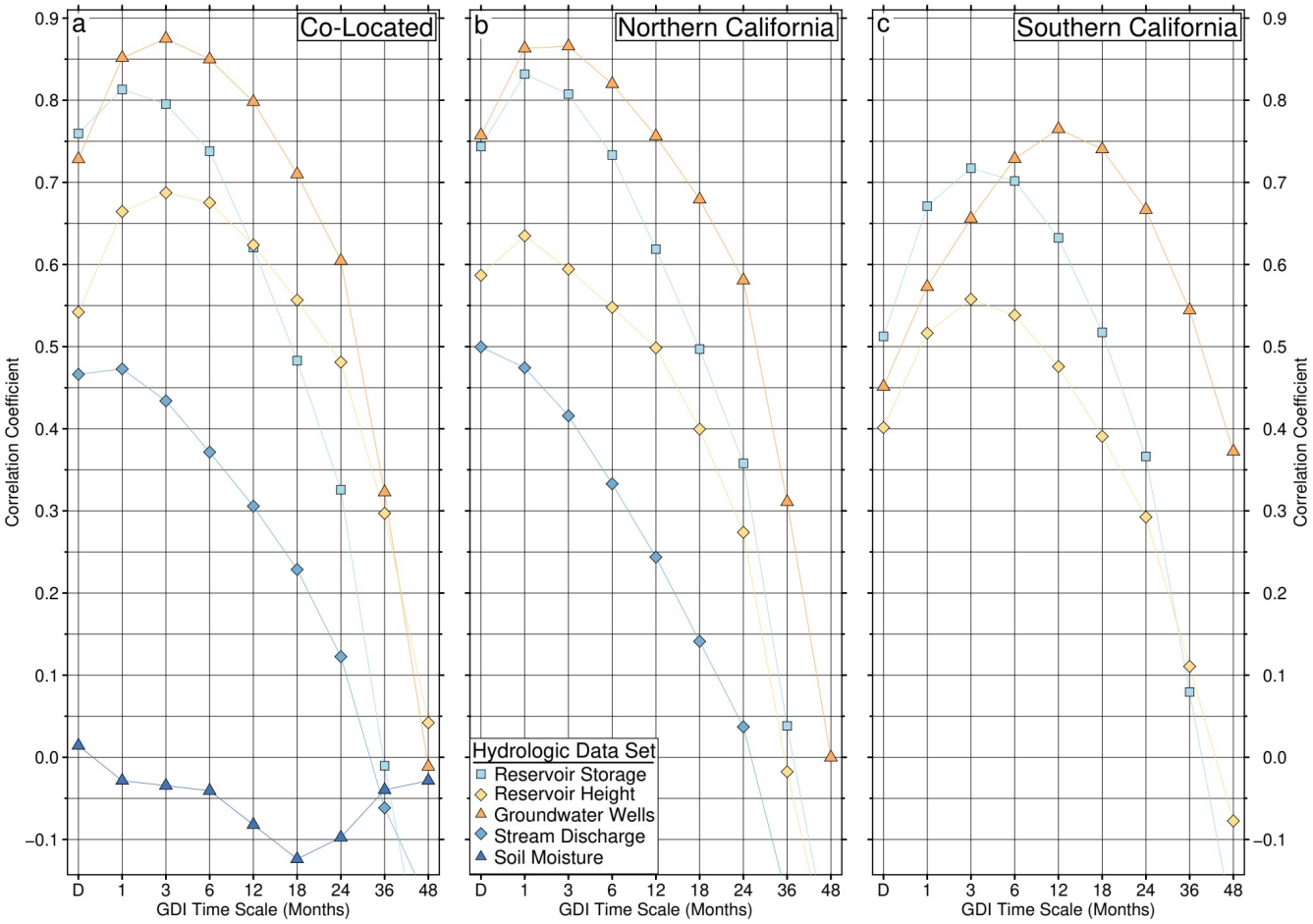

Figure 4: Correlation coefficients between (i) time series of the median GDI for each time scale and (ii) time series of median daily indexed reservoir storage, groundwater wells, reservoir height, stream discharge, and soil moisture anomalies for the (a) co-located, (b) Northern California, and (c) Southern California cases. Values are summarized in Table 3. Two sigma uncertainties are ± 0.03 for all data points. Note that the x-axes are non-linear and given in units of months (i.e., 30.44 days, except for "D," which stands for "daily").

Table 3: Correlation coefficients between the median GDI at various time scales and the daily indexed reservoir storage, groundwater wells, reservoir height, stream discharge, and soil moisture anomalies for the local, northern California, and southern California cases. Values are plotted in Figure 4. Two sigma uncertainties are ± 0.03. *Note that time scales are given in months with the exception of "D", which stands for "daily". Bold values indicate optimal GDI time scales for each hydrologic data set.

GDI Time Scale	**D***	**1**	**3**	**6**	**12**	**18**	**24**	**36**	**48**	

(Months)										
Hydrologic Observations	**Co-Located**									**Available Stations**
Groundwater Wells	0.73	0.85	**0.88**	0.85	0.80	0.71	0.60	0.32	−0.01	193
Reservoir Storage	0.76	**0.81**	0.80	0.74	0.62	0.48	0.33	−0.01	−0.30	72
Reservoir Height	0.54	0.66	**0.69**	0.68	0.62	0.56	0.48	0.30	0.04	20
Stream Discharge	**0.47**	**0.47**	0.43	0.37	0.31	0.23	0.12	−0.06	−0.18	70
Soil Moisture	0.01	−0.03	−0.03	−0.04	−0.08	−0.12	−0.10	-0.04	−0.03	11
Northern California										
Groundwater Wells	0.76	0.86	**0.87**	0.82	0.76	0.68	0.58	0.31	0.00	155
Reservoir Storage	0.74	**0.83**	0.81	0.73	0.62	0.50	0.36	0.04	−0.24	58
Reservoir Height	0.59	**0.63**	0.59	0.55	0.50	0.40	0.27	−0.02	−0.25	9
Stream Discharge	**0.50**	0.47	0.42	0.33	0.24	0.14	0.04	−0.17	−0.30	62
Soil Moisture	~	~	~	~	~	~	~	~	~	6
Southern California										
Groundwater Wells	0.45	0.57	0.66	0.73	**0.77**	0.74	0.67	0.54	0.37	29
Reservoir Storage	0.51	0.67	**0.72**	0.70	0.63	0.52	0.37	0.08	−0.20	13
Reservoir Height	0.40	0.52	**0.56**	0.54	0.48	0.39	0.29	0.11	−0.08	9
Stream Discharge	~	~	~	~	~	~	~	~	~	0
Soil Moisture	~	~	~	~	~	~	~	~	~	2

489

Time series of the 3-month, 1-month, and daily GDI for northern California are plotted in Figure 5, and overlain with the daily indexed groundwater wells, reservoir storage and stream discharge anomaly time series. Shaded regions reflect the inter-quartile range (IQR) for each data set. Figure 6 shows a similar comparison for southern California except that it shows the 12-month and 3-month GDI in comparison with the daily indexed groundwater wells and reservoir storage anomalies. Similarly, Figure S2 shows the optimal GDI for the co-located case.

Long-term trends of the GDI closely follow the hydrologic observations, with consistent overlap of the IQRs for most of the study period in both northern and southern California. In northern California, clusters of AR events (gray vertical lines) coincide with rapid increases in indices associated with the hydrological data. Concurrently, sharp increases in the GDI often initiate during AR sequences and closely follow the trends of the hydrologic observations, with a lag that ranges between a few weeks to several months. This is particularly evident between November 2015 and January 2017, during which two large clusters of ARs coincide with large increases in the GDI, from extreme hydrologic drought in November 2015 to extremely high hydrologic storage by February 2017.

Although fewer category 3+ ARs occur within the southern California region, we see a similar relationship when comparing the 3-month GDI with reservoir storage. The association diminishes, however, when comparing the daily groundwater index with the 12-month GDI. Nevertheless, a comparison of groundwater wells between northern and southern California shows clearly that groundwater fluctuations in southern California tend to evolve more slowly than groundwater fluctuations in northern California.

Some discrepancies are expected between the time series of hydrologic observations and the GDI (Figures 5, 6 and S2), because the GDI is driven by the response of the GPS observations across the entire region, while the hydrologic observations are point observations that are limited in both station quantity and spatial distribution. Larger deviations are observed in southern California, where far fewer hydrologic observations are available. Thus, due to the significant quantity of GPS stations in the region, compared to the quantity and distribution of hydrologic observations, the GDI results provide more significant insight into the regional hydrologic trends than can be observed with the current network of hydrologic stations.

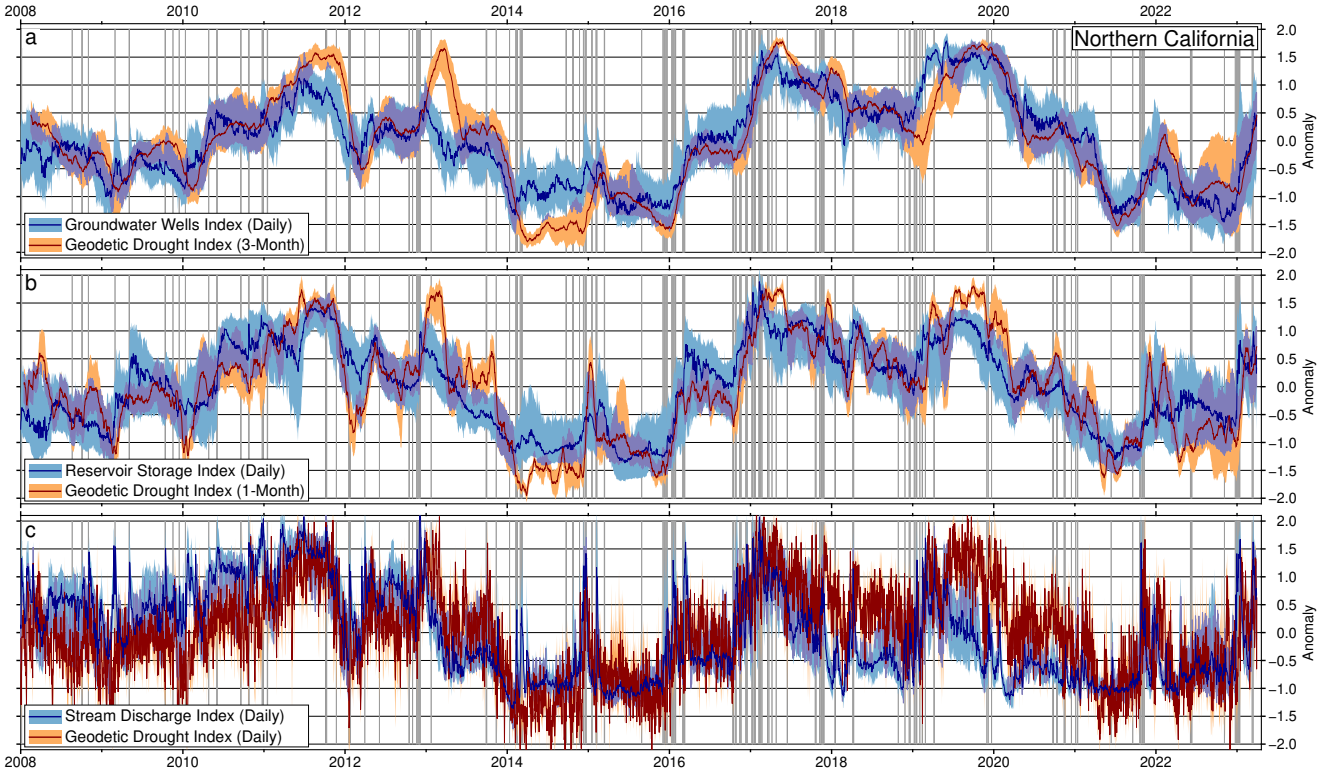

Figure 5: Time series comparison of GDI time scales and daily indexed hydrologic anomalies within northern California (Figure 2). (a) Comparison between the daily groundwater wells anomaly and the optimal 3-month GDI. The blue and red lines indicate the median index value, for each epoch, of the daily groundwater wells index and the 3-month GDI respectively (Figure 4). The light blue and orange shaded regions indicate the inter-quartile range for each index. (b) The same as panel a except comparing the daily reservoir storage anomaly with the optimal 1-month GDI. (c) The same as panel a except comparing the daily stream discharge anomaly with the optimal daily GDI. Grey vertical bars indicate category 3+ atmospheric river (AR) events in northern California.

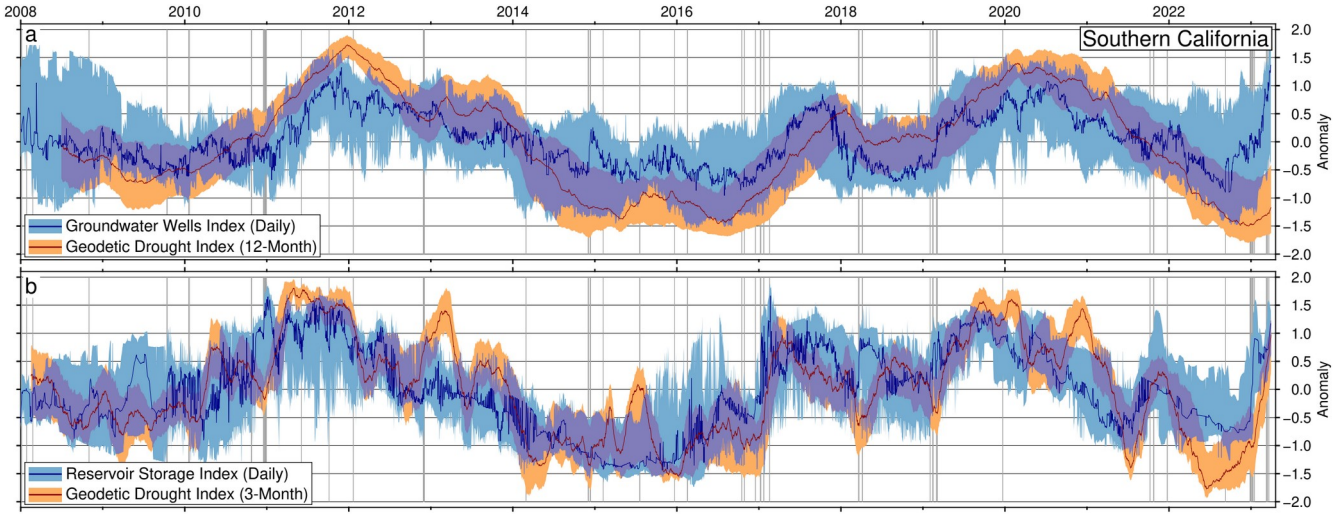

Figure 6: Time series comparison of GDI time scales and daily indexed hydrologic anomalies within southern California (Figure 1). (a) Comparison between the daily groundwater wells anomaly and the optimal 12-month GDI (Figure 4). (b) The same as panel a except comparing the daily reservoir storage anomaly with the optimal 3-month GDI. Key as described in Figure 5 with the exception that atmospheric river (AR) events are limited to southern California.

5 DISCUSSION

5.1 IMPROVING TWS MONITORING

The methods presented in this study leverage the sensitivities of hydrogeodesy and combine them with rigorously tested drought characterization techniques, to provide insight into regional TWS variation and comprehensive hydrological drought anomalies. Direct quantification of regional water storage, in both surface and subsurface reservoirs, has been difficult to perform in the past due to sparse spatial distributions of hydrologic data sets (Figure S1), the point-measurement nature of traditional hydrological observations, and the difficulty of observing groundwater. Furthermore, variations in groundwater well observations are strongly affected by aquifer dynamics (e.g. spatial heterogeneity), making comparisons difficult to quantify, even between neighboring wells. Hence, drought monitoring has historically relied heavily on meteorologic observations to assess drought intensity (along with streamflow observations, etc) to influence decisions regarding resource allocation, rather than incorporating or relying on direct hydrologic observations or TWS estimates (Svoboda et al., 2002; Svoboda & Fuchs, 2016).

While meteorological data provide important insight into the amount of water entering a watershed, meteorologic-based drought indices lack the ability to characterize anomalies in TWS, including groundwater storage. Geodesy allows scientists and drought assessment practitioners to characterize storage changes not only at the surface, but also in deep subsurface reservoirs, which provide critical water resources to communities and account for a large proportion of TWS. While alternative methods and data sets, such as GRACE-based drought indices, have been developed to address this problem, their ability to resolve TWS anomalies at fine spatial scales is limited. Furthermore, GRACE-based metrics are divorced from on-the-ground observation networks, which can expand and improve over time in station density and spatial extent.

In addition, intensities of meteorologic and hydrologic drought are rarely equivalent with variation in hydrologic drought lagging meteorologic drought due to runoff, evapotranspiration, and the time scales of drainage basin dynamics and aquifer recharge (Barker et al., 2016; Entekhabi et al., 1992; Lin et al., 2023; Werth et al., 2023). In other words, the unique behaviors and geographic contexts of each watershed affect TWS and hydrological drought, but do not impact meteorological assessments of drought. Furthermore, evaluating differences between hydrological and meteorological drought can be important for water-resource management, since improving the understanding of how TWS varies both spatially and over time can improve relevance and accuracy of drought-management

decisions, resulting in better resource sustainability through periods of prolonged drought. Continued expansion of GPS networks, particularly in sparsely monumented regions, and maintaining the operation of long running GPS stations will further improve TWS characterization.

5.2 GDI TIME SCALES AND HYDROLOGIC OBSERVATIONS

The vertical and horizontal displacements of Earth's surface observed by GPS represent the confluence of all sources of loading over short and long periods (and local to global scales). Thus, by adjusting the time scales over which we compute the GDI, the GPS-inferred estimates of TWS are summarized to emphasize various components of the total deformation signal. The time scales of hydrologic loading and unloading vary depending on the reservoir (e.g., groundwater versus stream discharge); thus, applying the GDI at different time scales provides insight into the behavior of different hydrological systems (Skøien et al., 2003).

As shown in Figure 4, we observe the strongest correlations between the GDI and stream discharge, at the daily to 1-month time scale, for which stream discharge fluctuates predominantly at weekly to monthly time scales. Reservoirs, that are fed from broader drainage basins exhibit longer characteristic time scales of one to three months. Intriguingly, we find different responses to groundwater well observations when distinguishing northern and southern California, with northern California exhibiting optimal correlations at the 1- to 3-month time scale, and southern California at the 12-month time scale. The peak correlation between GDI and groundwater at the longer (several month) time scales is not surprising considering that the shallow subsurface acts as a low pass filter of meteorological inputs, attenuating and dampening the comparatively high frequency forgings observed at the soil surface. Furthermore, spatial differences (e.g. north versus south here) may be representative of variations in groundwater aquifer characteristics including material properties and anthropogenic effects. Thus, time scales of 1- to 3- months in northern California (primarily driven by northern Central Valley wells) are likely to reflect a combination of agricultural pumping and recharge driven by precipitation and snowpack in the Sierra Nevada mountains (Werth et al., 2023). Moreover, the longer 12-month time scale in southern California (driven by Coastal Basin aquifer wells) are likely to reflect a greater dependence on natural aquifer recharge dynamics rather than agricultural effects.

Notably, excluding soil moisture, the optimal GDI time scales are sharply defined, with the correlation coefficients declining rapidly away from their peak. The strong associations suggest that, within northern California, the daily, 1-month, and 3-month GDIs are strong predictors of stream

discharge, reservoir storage/height, and groundwater wells, respectively. Similarly, the 3-month and 12-month GDIs are strong predictors of reservoir storage/height and groundwater wells in southern California.

As exemplified by the differences between northern and southern California, optimal GDI time scales are specific to each study region. The behaviors of hydrological systems vary depending on a variety of factors, including geological setting, regional ecology, and regional climate. Lorenzo-Lacruz et al. (2010), for example, found that the relationships of SPEI and SPI to hydrologic observations in Spain varied significantly across regions due to characteristics of individual drainage basins and the efficiency of groundwater flow through bedrock. Future work should consider mapping these differences in optimal timescales for groundwater to aide in operational assessments using the GDI.

The lack of a relationship between soil moisture and the GDI is not particularly surprising when considering its comparatively small hydrologic scale, which is often relatively thin (soils typically represent depths of meters while deeper groundwater aquifers can exceed 100s of meters). In addition, the dependence of the soil moisture data on the properties of both the soil layers and the topography suggests that significantly more soil moisture stations would be required to associate regional trends observed by the GDI with soil moisture observations.

5.3 LIMITATIONS OF A GPS-BASED GDI

A limitation of the GDI is the dependence on long-running, continuously operating GPS stations. For the study presented here, we have access to a large network of continuous GPS stations in the western United States for a period of nearly two decades. The density of stations and the long data records enable a robust analysis of several wet and dry cycles, which is not yet possible in many regions of the world. Dense networks operating over long periods enhances the ability of the GDI to recover more localized signals and mitigates bias in the solution.

Relatively long data records are important for calibrating the drought anomalies. Consider, for example, a network of GPS stations that is installed at the beginning of a drought period but discontinued at the end of the drought. The reference level of dryness for the region would be in the middle of the drought, which would bias the GDI to characterize the early period as relatively wet, despite the period being relatively dry in the context of longer observational periods, which are readily available for meteorologically based drought indices. Therefore, the period of record represented by any given network is an important consideration when conducting drought assessments. The GPS

constellation, however, will continue to operate for the foreseeable future, continuously increasing the length of data records. Thus, with time, and with the expansion of other GNSS worldwide, the limitation of short data records for the GDI will be reduced, but the effects of climate change may need to be considered in drought characterization in the future (Hoylman et al., 2022).

Short data records can also pose challenges for compiling distributions of wet and dry anomalies, upon which the GDI is based. We address this challenge by characterizing each epoch relative to a compiled distribution of nearby epochs rather than limiting the distribution to include only individual dates. By using an expanded window of ±15 days, we bolster the distribution significantly, to provide more robust (and stable) drought characterization. Thus, we can address the current limitation of short data records, and reduce the expanded windows over time as GPS time series extend.

5.4 THE INCLUSION OF HORIZONTAL COMPONENTS IN THE GPS INVERSION FOR TWS

In this study, we explore the impact of horizontal GPS components on TWS estimates and the GDI, with the goal of improving hydrologic load localization. Figure S3 provides a comparison of estimated TWS on 01 January 2023 for both the three-dimensional and vertical-only solutions. We select this date because it immediately follows three large AR events (category 3+) that generated large loading signals in the GPS. Comparison between the difference in these solutions with the cumulative precipitation over the four previous days, reveals higher load estimates downstream from the peak cumulative precipitation. While we observe short-term improved load localization during extreme precipitation events, we find that differences between a vertical-only solution and a three-dimensional solution are relatively small when considering the full study period. Moreover, the overall conclusions of this study are identical whether we include horizontal GPS components or not. We interpret the relative insignificance of the horizontal components to be due to the relative strength of the vertical signal, as well as the relative (i.e., anomaly) nature of the GDI. Except for extreme precipitation events (Figure S3), we find that including the horizontal components shifts loads slightly between neighboring grid cells, but the small spatial shifts become mostly irrelevant in the GDI framework due to normalization. Thus, for simplicity and due to negligible benefits, we conclude that it is reasonable to omit horizontal components from a GDI analysis at current GPS observational precision. The relative importance of horizontal components, however, should be reevaluated in the future, since improvements in technology and the inclusion of multiple satellite networks in GNSS positioning could enhance the benefits of including horizontals in due course.

6 CONCLUSIONS

In this study, we present new insights into geodetic drought indices (GDI), including advances in the computation of the GDI, an assessment of optimal GDI time scales that correlate strongly with key components of hydrological systems in California, and an evaluation of GDI response to heavy precipitation associated with atmospheric rivers. We build upon the methods of Chew & Small (2014), Tang et al. (2023), and others to derive the multi-scale GPS-based GDI and we evaluate its ability to characterize specific hydrologic reservoirs and fluxes that are of interest to water-resource managers.

Comparison between northern and southern California reveals that the GDI identifies different optimal time scales to accurately characterize groundwater dynamics within each region, providing insight into the physical processes that drive hydrologic variation. In northern California, the GDI effectively characterizes groundwater wells, reservoir storage, reservoir height, and stream discharge at the 3-month, 1-month, 1-month, and daily time scales, respectively, with correlation coefficients of 0.87, 0.83, 0.63, and 0.50. In southern California, groundwater wells, reservoir storage, and reservoir height are best represented by longer GDI time scales of 12-, 3- and 3-months, respectively, with correlation coefficients of 0.77, 0.72, and 0.56. Correlation coefficients between the GDI and fluctuations in the hydrological systems peak strongly at single time scales and taper off rapidly at both shorter and longer time scales. We therefore infer that the GDI, tailored to a specific region and time scale, can be a strong predictor of variations in lakes and reservoirs, stream discharge, and groundwater. We find, however, no clear association between the GDI and soil-moisture changes at any time scale indicating the GDI is most sensitive to TWS (of which groundwater is a comparatively large component).

Moreover, we find that heavy precipitation events associated with atmospheric rivers affect both the hydrologic observations and the GDI at short periods. Thus, we demonstrate that the GDI is sensitive to both short- and long-term variations in TWS, characteristics of specific hydrologic basins, and specific hydrologic reservoirs (e.g., groundwater and reservoir storage).

Despite growing interest in, and advances in the development of GDIs, over the past decade (Chew & Small, 2014; Ferreira et al., 2018; Jiang et al., 2022a; Jiang et al., 2022b; Tang et al., 2023), GDIs are not currently incorporated in active drought management. We strongly advocate for the integration of GDIs into routine drought monitoring and assessment. The methods that we present here to compute the GPS-based GDI are readily scalable to other geodetic networks and regions worldwide.

691 The use of GDIs can provide water-resource managers with regular (e.g., daily) insights into
692 hydrological drought conditions not only regionally but also with respect to individual drainage basins,
693 and specific hydrologic reservoirs. Importantly, the GDI presents opportunities for monitoring
694 groundwater anomalies, which has historically been an underrepresented indicator of long-term drought
695 dynamics. Future work should advance this framework into an operational context to aid in more
696 holistic drought assessments.

ACKNOWLEDGMENTS

This material is based upon work supported by the National Science Foundation under Grant number 2021637.

DATA AND RESOURCES

The GPS data and the initial steps catalog used in this study are available from the Nevada Geodetic Laboratory at http://geodesy.unr.edu [Blewitt et al., (2018); last accessed April 2023]. The LoadDef software is available at https://www.github.com/hrmartens/LoadDef [Martens et al., (2019); last accessed April 2023]. Hydrologic data for groundwater wells, reservoir storage, reservoir/lake height, and stream discharge are available from the National Water Information System at https://nwis.waterdata.usgs.gov/nwis (last accessed April 2023). We provide the soil-moisture data used in this study at https://doi.org/10.5281/zenodo.8403730. The atmospheric rivers catalog is available via ftp://sioftp.ucsd.edu/CW3E_DataShare/Rutz_AR_Catalog/ (last accessed August 2023). Non-tidal atmospheric and oceanic loading data is available from GFZ-Potsdam at http://rz-vm115.gfz-potsdam.de:8080/repository/entry/show?entryid=24aacdfe-f9b0-43b7-b4c4-bdbe51b6671b (last accessed April 2023).

715 **REFERENCES**

Ahmad, S. K., Kumar, S. V., Lahmers, T. M., Wang, S., Liu, P.-W., Wrzesien, M. L., et al. (2022). Flash Drought Onset and Development Mechanisms Captured With Soil Moisture and Vegetation Data Assimilation. *Water Resources Research*, *58*(12), e2022WR032894. https://doi.org/10.1029/2022WR032894

Altamimi, Z., Rebischung, P., Métivier, L., & Collilieux, X. (2016). ITRF2014: A new release of the International Terrestrial Reference Frame modeling nonlinear station motions. *Journal of Geophysical Research: Solid Earth*, *121*(8), 6109–6131. https://doi.org/10.1002/2016JB013098

Amos, C. B., Audet, P., Hammond, W. C., Bürgmann, R., Johanson, I. A., & Blewitt, G. (2014). Uplift and seismicity driven by groundwater depletion in central California. *Nature*, *509*(7501), 483–486. https://doi.org/10.1038/nature13275

Argus, D. F., Fu, Y., & Landerer, F. W. (2014). Seasonal variation in total water storage in California inferred from GPS observations of vertical land motion. *Geophysical Research Letters*, *41*(6), 1971–1980. https://doi.org/10.1002/2014GL059570

Argus, D. F., Landerer, F. W., Wiese, D. N., Martens, H. R., Fu, Y., Famiglietti, J. S., et al. (2017). Sustained Water Loss in California's Mountain Ranges During Severe Drought From 2012 to 2015 Inferred From GPS. *Journal of Geophysical Research: Solid Earth*, *122*(12), 10,559-10,585. https://doi.org/10.1002/2017JB014424

Aster, R. C., & Thurber, C. H. (2013). *Parameter estimation and inverse problems* (2nd ed). Waltham, MA: Academic Press.

Barker, L. J., Hannaford, J., Chiverton, A., & Svensson, C. (2016). From meteorological to hydrological drought using standardised indicators. *Hydrology and Earth System Sciences*, *20*(6), 2483–2505. https://doi.org/10.5194/hess-20-2483-2016

Bertiger, W., Bar-Sever, Y., Dorsey, A., Haines, B., Harvey, N., Hemberger, D., et al. (2020). GipsyX/RTGx, a new tool set for space geodetic operations and research. *Advances in Space Research*, *66*(3), 469–489. https://doi.org/10.1016/j.asr.2020.04.015

Blewitt, G., Hammond, W., & Kreemer, C. (2018). Harnessing the GPS Data Explosion for Interdisciplinary Science. *Eos*, *99*. https://doi.org/10.1029/2018EO104623

Borsa, A. A., Agnew, D. C., & Cayan, D. R. (2014). Ongoing drought-induced uplift in the western United States. *Science*, *345*(6204), 1587–1590. https://doi.org/10.1126/science.1260279

California Data Exchange Center. (2023). CDEC Webservice JSON and CSV. Retrieved June 21, 2023, from https://cdec.water.ca.gov/dynamicapp/wsSensorData

California Natural Resources Agency. (2023a). Continuous Groundwater Level Measurements. Retrieved 27 December 2023. https://data.cnra.ca.gov/dataset/continuous-groundwater-level-measurements

California Natural Resources Agency. (2023b). Periodic Groundwater Level Measurements. Retrieved 27 December 2023. https://data.cnra.ca.gov/dataset/periodic-groundwater-level-measurements

Chew, C. C., & Small, E. E. (2014). Terrestrial water storage response to the 2012 drought estimated from GPS vertical position anomalies. *Geophysical Research Letters*, *41*(17), 6145–6151. https://doi.org/10.1002/2014GL061206

Dill, R., & Dobslaw, H. (2013). Numerical simulations of global-scale high-resolution hydrological crustal deformations. *Journal of Geophysical Research: Solid Earth*, *118*(9), 5008–5017. https://doi.org/10.1002/jgrb.50353

Entekhabi, D., Rodriguez-Iturbe, I., & Bras, R. L. (1992). Variability in Large-Scale Water Balance with Land Surface-Atmosphere Interaction. *Journal of Climate*, *5*(8), 798–813. https://doi.org/10.1175/1520-0442(1992)005<0798:VILSWB>2.0.CO;2

Famiglietti, J. S. (2014). The global groundwater crisis. *Nature Climate Change*, *4*(11), 945–948. https://doi.org/10.1038/nclimate2425

Ferreira, V. G., Montecino, H. C., Ndehedehe, C. E., Heck, B., Gong, Z., de Freitas, S. R. C., & Westerhaus, M. (2018). Space-based observations of crustal deflections for drought characterization in Brazil. *Science of The Total Environment*, *644*, 256–273. https://doi.org/10.1016/j.scitotenv.2018.06.277

Ford, T. W., Wang, Q., & Quiring, S. M. (2016). The Observation Record Length Necessary to Generate Robust Soil Moisture Percentiles. *Journal of Applied Meteorology and Climatology*, *55*(10), 2131–2149. https://doi.org/10.1175/JAMC-D-16-0143.1

Fu, Y., Argus, D. F., Freymueller, J. T., & Heflin, M. B. (2013). Horizontal motion in elastic response to seasonal loading of rain water in the Amazon Basin and monsoon water in Southeast Asia observed by GPS and inferred from GRACE: HORIZONTAL SEASONAL MOTIONS BY GPS/GRACE. *Geophysical Research Letters*, *40*(23), 6048–6053. https://doi.org/10.1002/2013GL058093

Fu, Y., Argus, D. F., & Landerer, F. W. (2015). GPS as an independent measurement to estimate terrestrial water storage variations in Washington and Oregon. *Journal of Geophysical Research: Solid Earth*, *120*(1), 552–566. https://doi.org/10.1002/2014JB011415

He, X., Wada, Y., Wanders, N., & Sheffield, J. (2017). Intensification of hydrological drought in California by human water management. *Geophysical Research Letters*, *44*(4), 1777–1785. https://doi.org/10.1002/2016GL071665

Houborg, R., Rodell, M., Li, B., Reichle, R., & Zaitchik, B. F. (2012). Drought indicators based on model-assimilated Gravity Recovery and Climate Experiment (GRACE) terrestrial water storage observations. *Water Resources Research*, *48*(7). https://doi.org/10.1029/2011WR011291

Hoylman, Z. H., Bocinsky, R. K., & Jencso, K. G. (2022). Drought assessment has been outpaced by climate change: empirical arguments for a paradigm shift. *Nature Communications*, *13*(1), 2715. https://doi.org/10.1038/s41467-022-30316-5

Jiang, Z., Hsu, Y.-J., Yuan, L., Tang, M., Yang, X., & Yang, X. (2022a). Hydrological drought characterization based on GNSS imaging of vertical crustal deformation across the contiguous United States. *Science of The Total Environment*, *823*, 153663. https://doi.org/10.1016/j.scitotenv.2022.153663

Jiang, Z., Hsu, Y.-J., Yuan, L., Cheng, S., Feng, W., Tang, M., & Yang, X. (2022b). Insights into hydrological drought characteristics using GNSS-inferred large-scale terrestrial water storage

deficits. *Earth and Planetary Science Letters*, *578*, 117294. https://doi.org/10.1016/j.epsl.2021.117294

Jones, K. A., Niknami, L. S., Buto, S. G., & Decker, D. (2022). *Federal standards and procedures for the National Watershed Boundary Dataset (WBD): Chapter 3 of Section A, Federal Standards, Book 11, Collection and Delineation of Spatial Data* (USGS Numbered Series No. 11-A3). *Federal standards and procedures for the National Watershed Boundary Dataset (WBD): Chapter 3 of Section A, Federal Standards, Book 11, Collection and Delineation of Spatial Data* (Vol. 11-A3, p. 54). Reston, VA: U.S. Geological Survey. https://doi.org/10.3133/tm11a3

Kang, S., & Knight, R. (2023). Isolating the Poroelastic Response of the Groundwater System in InSAR Data From the Central Valley of California. *Geophysical Research Letters*, *50*(9), e2023GL103222. https://doi.org/10.1029/2023GL103222

Knappe, E., Bendick, R., Martens, H. R., Argus, D. F., & Gardner, W. P. (2019). Downscaling Vertical GPS Observations to Derive Watershed-Scale Hydrologic Loading in the Northern Rockies. *Water Resources Research*, *55*(1), 391–401. https://doi.org/10.1029/2018WR023289

Larochelle, S., Chanard, K., Fleitout, L., Fortin, J., Gualandi, A., Longuevergne, L., et al. (2022). Understanding the Geodetic Signature of Large Aquifer Systems: Example of the Ozark Plateaus in Central United States. *Journal of Geophysical Research: Solid Earth*, *127*(3), e2021JB023097. https://doi.org/10.1029/2021JB023097

Laveti, N. V. S., Banerjee, A., Kartha, S. A., & Dutta, S. (2021). Anthropogenic influence on monthly groundwater utilization in an irrigation dominated Ganga river Sub-Basin. *Journal of Hydrology*, *593*, 125800. https://doi.org/10.1016/j.jhydrol.2020.125800

Li, B., Rodell, M., Kumar, S., Beaudoing, H. K., Getirana, A., Zaitchik, B. F., et al. (2019). Global GRACE Data Assimilation for Groundwater and Drought Monitoring: Advances and Challenges. *Water Resources Research*, *55*(9), 7564–7586. https://doi.org/10.1029/2018WR024618

Lin, Q., Wu, Z., Zhang, Y., Peng, T., Chang, W., & Guo, J. (2023). Propagation from meteorological to hydrological drought and its application to drought prediction in the Xijiang River basin, South China. *Journal of Hydrology*, *617*, 128889. https://doi.org/10.1016/j.jhydrol.2022.128889

Liu, P.-W., Famiglietti, J. S., Purdy, A. J., Adams, K. H., McEvoy, A. L., Reager, J. T., et al. (2022). Groundwater depletion in California's Central Valley accelerates during megadrought. *Nature Communications*, *13*(1), 7825. https://doi.org/10.1038/s41467-022-35582-x

Martens, H. R., Rivera, L., & Simons, M. (2019). LoadDef: A Python-Based Toolkit to Model Elastic Deformation Caused by Surface Mass Loading on Spherically Symmetric Bodies. *Earth and Space Science*, *6*(2), 311–323. https://doi.org/10.1029/2018EA000462

Medellín-Azuara, J., Escriva-Bou, A., Rodríguez-Flores, J. M., Cole, S. A., Abatzoglou, J. T., Viers, J. H., et al. (2022). *Economic Impacts of the 2020-2022 Drought on California Agriculture* (A report for the California Department of Food and Agriculture.) (p. 35). Water Systems Management Lab. University of California, Merced. Retrieved from https://wsm.ucmerced.edu/wp-content/uploads/2023/01/Economic_Impact_CA_Drought_V02-1.pdf

Mishra, A. K., & Singh, V. P. (2010). A review of drought concepts. *Journal of Hydrology*, *391*(1), 202–216. https://doi.org/10.1016/j.jhydrol.2010.07.012

Otkin, J. A., Svoboda, M., Hunt, E. D., Ford, T. W., Anderson, M. C., Hain, C., & Basara, J. B. (2018). Flash Droughts: A Review and Assessment of the Challenges Imposed by Rapid-Onset Droughts in the United States. *Bulletin of the American Meteorological Society*, *99*(5), 911–919. https://doi.org/10.1175/BAMS-D-17-0149.1

Overacker, J., Hammond, W. C., Blewitt, G., & Kreemer, C. (2022). Vertical Land Motion of the High Plains Aquifer Region of the United States: Effect of Aquifer Confinement Style, Climate Variability, and Anthropogenic Activity. *Water Resources Research*, *58*(6), e2021WR031635. https://doi.org/10.1029/2021WR031635

Palmer, W. C. (1965). *Meteorological Drought*. U.S. Department of Commerce, Weather Bureau.

Prein, A. F., Holland, G. J., Rasmussen, R. M., Clark, M. P., & Tye, M. R. (2016). Running dry: The U.S. Southwest's drift into a drier climate state. *Geophysical Research Letters*, *43*(3), 1272–1279. https://doi.org/10.1002/2015GL066727

Rodell, M., Famiglietti, J. S., Wiese, D. N., Reager, J. T., Beaudoing, H. K., Landerer, F. W., & Lo, M.-H. (2018). Emerging trends in global freshwater availability. *Nature*, *557*(7707), 651–659. https://doi.org/10.1038/s41586-018-0123-1

Rutz, J. J., & Steenburgh, W. J. (2012). Quantifying the role of atmospheric rivers in the interior western United States. *Atmospheric Science Letters*, *13*(4), 257–261. https://doi.org/10.1002/asl.392

Rutz, J. J., Steenburgh, W. J., & Ralph, F. M. (2014). Climatological Characteristics of Atmospheric Rivers and Their Inland Penetration over the Western United States. *Monthly Weather Review*, *142*(2), 905–921. https://doi.org/10.1175/MWR-D-13-00168.1

Rutz, J. J., Shields, C. A., Lora, J. M., Payne, A. E., Guan, B., Ullrich, P., et al. (2019). The Atmospheric River Tracking Method Intercomparison Project (ARTMIP): Quantifying Uncertainties in Atmospheric River Climatology. *Journal of Geophysical Research: Atmospheres*, *124*(24), 13777–13802. https://doi.org/10.1029/2019JD030936

Singh, V. P., Guo, H., & Yu, F. X. (1993). Parameter estimation for 3-parameter log-logistic distribution (LLD3) by Pome. *Stochastic Hydrology and Hydraulics*, *7*(3), 163–177. https://doi.org/10.1007/BF01585596

Skøien, J. O., Blöschl, G., & Western, A. W. (2003). Characteristic space scales and timescales in hydrology. *Water Resources Research*, *39*(10). https://doi.org/10.1029/2002WR001736

Svoboda, M., & Fuchs, B. A. (2016). Handbook of Drought Indicators and Indices, *World Meteorological Organization (WMO) and Global Water Partnership (GWP)*.

Svoboda, Mark, LeComte, D., Hayes, M., Heim, R., Gleason, K., Angel, J., et al. (2002). THE DROUGHT MONITOR. *Bulletin of the American Meteorological Society*, *83*(8), 1181–1190. https://doi.org/10.1175/1520-0477-83.8.1181

Tang, M., Yuan, L., Jiang, Z., Yang, X., Li, C., & Liu, W. (2023). Characterization of hydrological droughts in Brazil using a novel multiscale index from GNSS. *Journal of Hydrology*, *617*, 128934. https://doi.org/10.1016/j.jhydrol.2022.128934

Thomas, B. F., Famiglietti, J. S., Landerer, F. W., Wiese, D. N., Molotch, N. P., & Argus, D. F. (2017). GRACE Groundwater Drought Index: Evaluation of California Central Valley groundwater drought. *Remote Sensing of Environment*, *198*, 384–392. https://doi.org/10.1016/j.rse.2017.06.026

U.S. Drought Monitor. (2023) Comprehensive Statistics. Retrieved 07 July 2023. https://droughtmonitor.unl.edu/DmData/DataDownload/ComprehensiveStatistics.aspx

U.S. Geological Survey. (2016). National Water Information System data available on the World Wide Web (USGS Water Data for the Nation). Retrieved May 17, 2023, from https://waterdata.usgs.gov/nwis

Vicente-Serrano, S. M., Beguería, S., & López-Moreno, J. I. (2010). A Multiscalar Drought Index Sensitive to Global Warming: The Standardized Precipitation Evapotranspiration Index. *Journal of Climate*, *23*(7), 1696–1718. https://doi.org/10.1175/2009JCLI2909.1

Water Data Library. (2023a). Continuous Data. Retrieved 27 December 2023. https://wdl.water.ca.gov/waterdatalibrary/ContinuousData.aspx

Water Data Library. (2023b). Groundwater Level Data. Retrieved 27 December 2023. https://wdl.water.ca.gov/waterdatalibrary/GroundWaterLevel.aspx

Wiese, D. N., Yuan, D.-N., Boening, C., Landerer, F. W., Watkins, M. M.. 2023. JPL GRACE and GRACE-FO Mascon Ocean, Ice, and Hydrology Equivalent Water Height JPL. Ver. RL06.1Mv03. PO.DAAC, CA, USA. Dataset accessed 2023-09-14 at https://doi.org/10.5067/TEMSC-3MJ63

Wells, N., Goddard, S., & Hayes, M. J. (2004). A Self-Calibrating Palmer Drought Severity Index. *Journal of Climate*, *17*(12), 2335–2351. https://doi.org/10.1175/1520-0442(2004)017<2335:ASPDSI>2.0.CO;2

Werth, S., Shirzaei, M., Carlson, G., & Bürgmann, R. (2023). *Linking Central Valley Deep Aquifer Recharge and High Sierra Nevada Snowpack* (preprint). Preprints. https://doi.org/10.22541/essoar.167870414.42808951/v1

White, A. M., Gardner, W. P., Borsa, A. A., Argus, D. F., & Martens, H. R. (2022). A Review of GNSS/GPS in Hydrogeodesy: Hydrologic Loading Applications and Their Implications for Water Resource Research. *Water Resources Research*, *58*(7), e2022WR032078. https://doi.org/10.1029/2022WR032078

Wilhite, D. A., Svoboda, M. D., & Hayes, M. J. (2007). Understanding the complex impacts of drought: A key to enhancing drought mitigation and preparedness. *Water Resources Management*, *21*(5), 763–774. https://doi.org/10.1007/s11269-006-9076-5

Williams, A. P., Cook, B. I., & Smerdon, J. E. (2022). Rapid intensification of the emerging southwestern North American megadrought in 2020–2021. *Nature Climate Change*, *12*(3), 232–234. https://doi.org/10.1038/s41558-022-01290-z

Wu, W.-Y., Lo, M.-H., Wada, Y., Famiglietti, J. S., Reager, J. T., Yeh, P. J.-F., et al. (2020). Divergent effects of climate change on future groundwater availability in key mid-latitude aquifers. *Nature Communications*, *11*(1), 3710. https://doi.org/10.1038/s41467-020-17581-y

Xiao, M., Koppa, A., Mekonnen, Z., Pagán, B. R., Zhan, S., Cao, Q., et al. (2017). How much groundwater did California's Central Valley lose during the 2012–2016 drought? *Geophysical Research Letters*, *44*(10), 4872–4879. https://doi.org/10.1002/2017GL073333

Young, Z. M., Kreemer, C., & Blewitt, G. (2021). GPS Constraints on Drought-Induced Groundwater Loss Around Great Salt Lake, Utah, With Implications for Seismicity Modulation. *Journal of Geophysical Research: Solid Earth*, *126*(10), e2021JB022020. https://doi.org/10.1029/2021JB022020

Young, Z. M., Kreemer, C., Hammond, W. C., & Blewitt, G. (2023). Interseismic Strain Accumulation between the Colorado Plateau and the Eastern California Shear Zone: Implications for the Seismic Hazard near Las Vegas, Nevada. *Bulletin of the Seismological Society of America*. https://doi.org/10.1785/0120220136

Zhao, M., A, G., Velicogna, I., & Kimball, J. S. (2017). A Global Gridded Dataset of GRACE Drought Severity Index for 2002–14: Comparison with PDSI and SPEI and a Case Study of the Australia Millennium Drought. *Journal of Hydrometeorology*, *18*(8), 2117–2129. https://doi.org/10.1175/JHM-D-16-0182.1

716

Supplemental Material for...

Drought Characterization with GPS: Insights into Groundwater and Reservoir Storage in California

Zachary M. Young[1], Hilary R. Martens[1], Zachary H. Hoylman[2], and W. Payton Gardner[1]

[1] Department of Geosciences, University of Montana, Missoula, MT, USA

[2] Montana Climate Office, W.A. Franke College of Forestry and Conservation, University of Montana, Missoula, MT, USA

1 SUPPLEMENTAL FIGURES

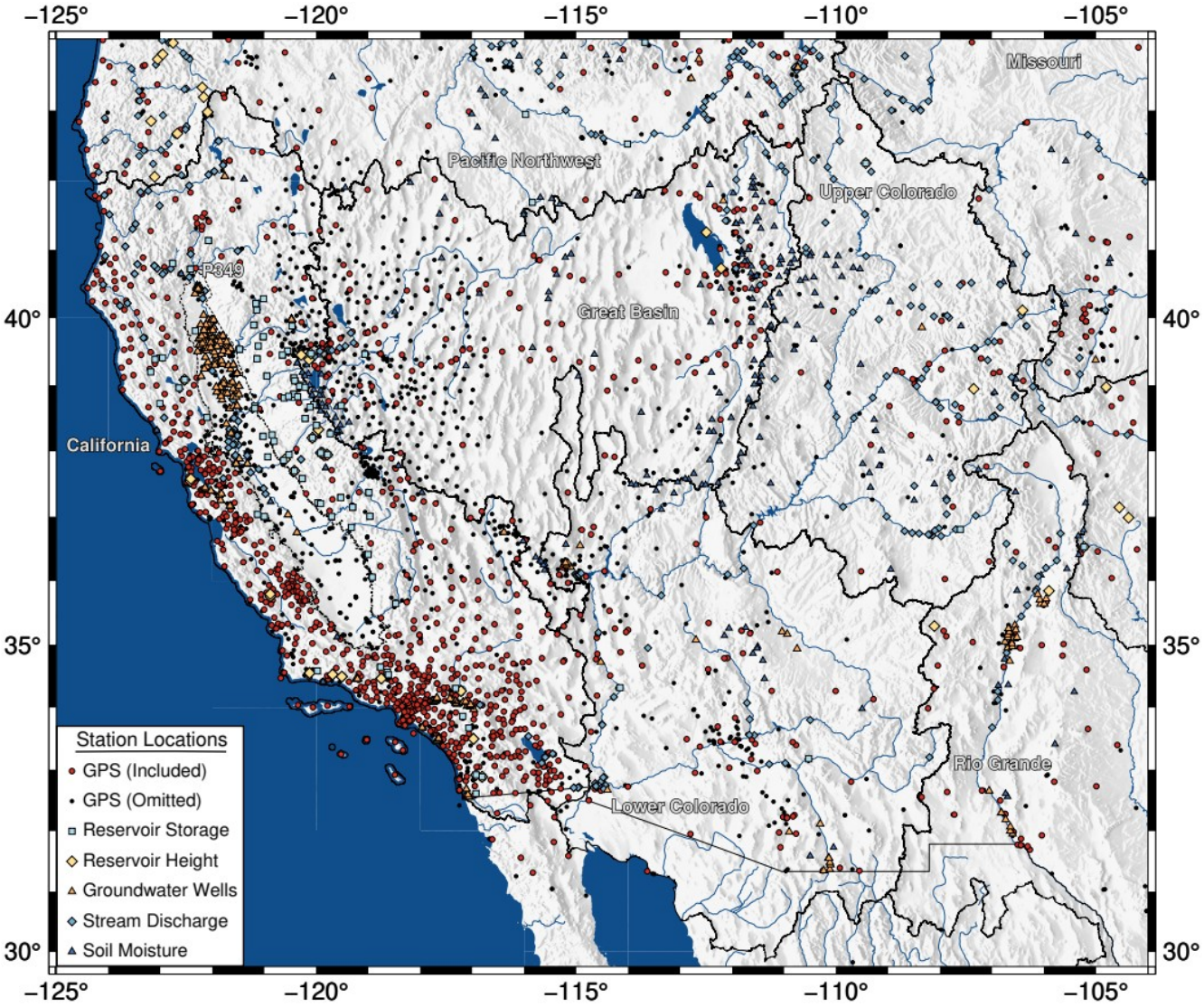

Figure S1: Expanded regional map showing the distribution of GPS and hydrologic stations considered in this study. Included GPS stations are shown as red circles while those omitted are presented as black dots. Reservoir storage locations are shown as light blue squares and lake/reservoir water surface height gauges are yellow diamonds. Groundwater wells are presented as orange triangles. Stream discharge gauges are shown as blue diamonds and soil moisture stations are identified as dark blue triangles. Labeled level two hydrologic unit code (HUC2) boundaries are shown as thick black lines (Jones et al., 2022). Blue lines show the location of rivers. The boundary for California's Central Valley is shown as a thin dashed black line. The location of GPS station P349, near Lake Shasta in northern California, is indicated with a black line from its label.

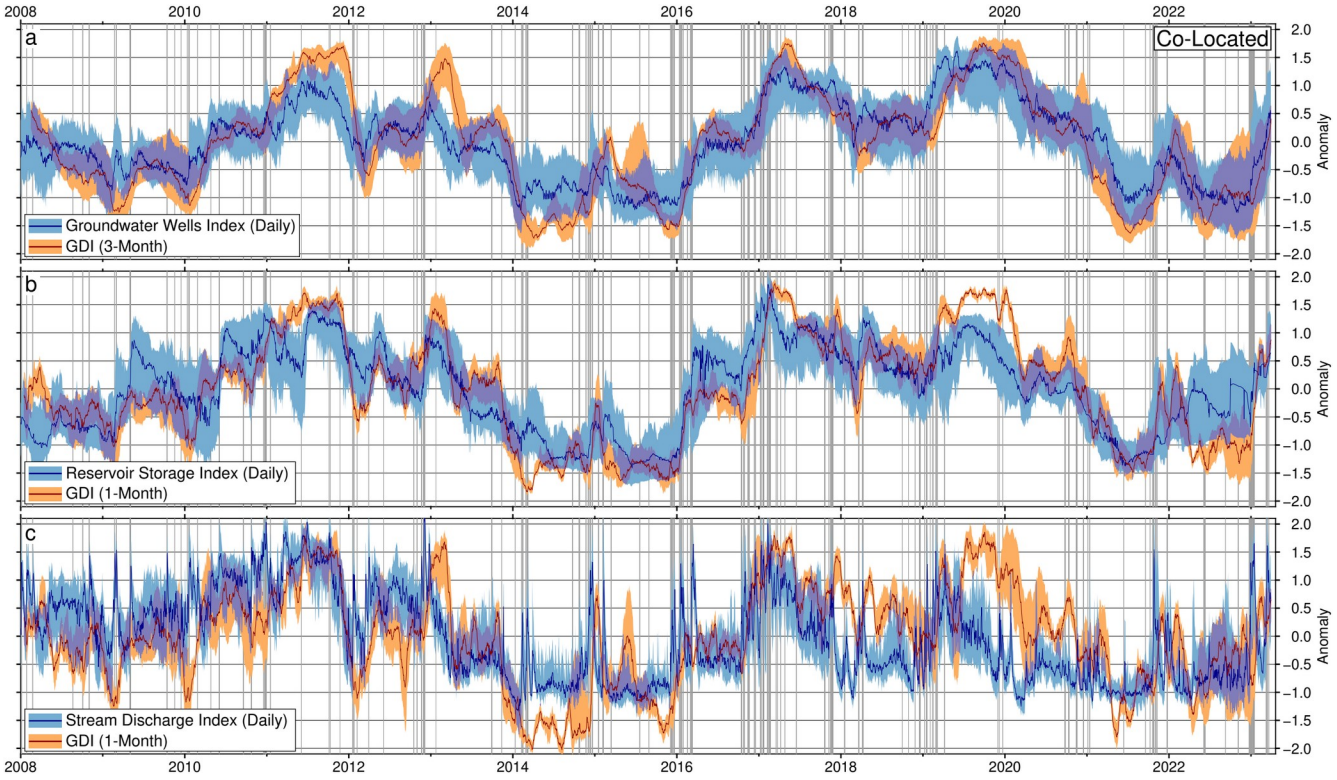

Figure S2: Comparison of co-located GDI time scales and daily indexed hydrologic anomalies (Figure 2). (a) Comparison between the daily groundwater wells anomaly and the optimal 3-month GDI (Figure 4). The blue and red lines indicate the median index value, for each epoch, of the daily groundwater wells index and the 3-month GDI respectively. The light blue and orange shaded regions indicate the inter-quartile range for each index. (b) The same as panel a except comparing the daily reservoir storage anomaly with the optimal 1-month GDI. (c) The same as panel a except comparing the daily stream discharge anomaly with the optimal 1-month GDI. Grey vertical bars indicate category 3+ atmospheric river (AR) events in northern and southern California.

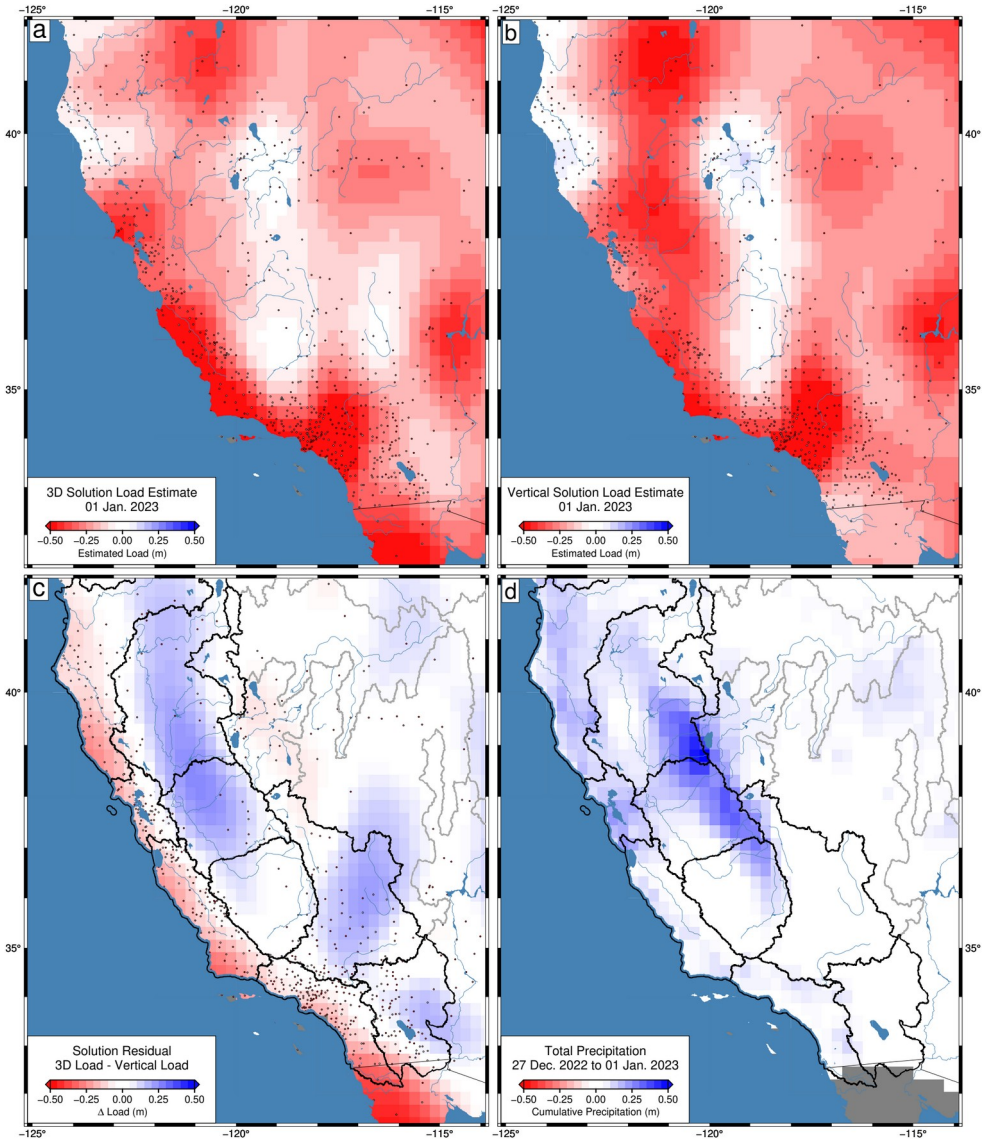

Figure S3: Comparison of 3-dimensional (3D) and vertical only load solutions. Hydrologic load estimates for the (a) 3D load and (b) vertical only load solution on 01 January 2023. Loads are presented relative to the full study period of 2008 to 2023. (c) Difference between the two load solutions (3D - vertical) presented in panels a and b. (d) Cumulative precipitation between 27 December 2022 and 01 January 2023. Black dots in panels a – c indicate GPS station locations used in the inversion. Black and grey lines denote hydrologic unit code level 4 boundaries for California and the Great Basin respectively. Between 27 December 2022 and 01 January 2023, northern California experienced three days of category 3+ atmospheric rivers. Blue lines represent the locations of rivers. Note that the highest cumulative precipitation occurs in the two hydrologic units which experience the largest increase in load for the 3D solution (localized toward to base of the drainage basin).

2 SUPPLEMENTAL TEXT

Text S1:

We analyzed a comprehensive database of daily soil moisture time-series sourced from federal and state networks, including SNOwpack TELemetry (SNOTEL), Soil Climate Analysis Network (SCAN), the U.S. Climate Reference Network (USCRN), and the Montana Mesonet. Our assessment encompassed 1,810 soil moisture time-series from 641 locations, wi1.1th volumetric soil moisture measurements at depths ranging from 2 to 40 inches below the ground surface. The time periods considered varied by site and extended from October 12, 1996, to December 19, 2022. To ensure data reliability, we filtered out periods when soil temperatures were below 1.1°C (34°F), indicating frozen soil. For this analysis we used soil moisture data recorded at the 20in depth.

We standardized each soil moisture time-series using a parametric approach, addressing non-Gaussian distributions within each site-specific time-series. Instead of relying solely on a single day (e.g., June 1st) to define the distribution for each year, we adopted a more robust method. Specifically, we employed a 31-day centered moving-window technique, which required a minimum of 6 years of data (equivalent to 6 years x 31 days, resulting in a minimum of 186 observations) to create samples for the site of interest. This approach aligns with the work of Ford et al. (2016), who utilized 31-day samples per year to estimate percentiles, concluding that 6 years of data is generally adequate for establishing stable and reliable percentiles for soil moisture. Essentially, our approach capitalizes on the natural cyclic and seasonal variations in soil moisture time-series, enhancing the probability distribution associated with any given day and location (e.g., conditions on May 31st offering insights into, and probabilistic information about, June 1st).

Subsequently, we applied a Gamma distribution to each specific day/location/depth sample, utilizing the L-moments of the data for estimating the corresponding probability distribution. We chose the Gamma distribution due to its capacity to accommodate non-Gaussian data that is constrained to a minimum of zero, aligning with the typical characteristics of soil moisture datasets. Employing these parametrically derived probability distributions, we computed the associated cumulative distribution function (CDF) for the observations. These CDF values were then subjected to evaluation within an inverse Gaussian function characterized by a mean of zero and a standard deviation of one, resulting in the ultimate anomaly value. This "normalization" procedure centers CDF values around 0.5, anchoring them to an anomaly value of zero.

3 SUPPLEMENTAL REFERENCES

Ford, T. W., Wang, Q., & Quiring, S. M. (2016). The observation record length necessary to generate robust soil moisture percentiles. *Journal of Applied Meteorology and Climatology*, *55*(10), 2131-2149.

Jones, K. A., Niknami, L. S., Buto, S. G., & Decker, D. (2022). *Federal standards and procedures for the National Watershed Boundary Dataset (WBD): Chapter 3 of Section A, Federal Standards, Book 11, Collection and Delineation of Spatial Data* (USGS Numbered Series No. 11-A3). *Federal standards and procedures for the National Watershed Boundary Dataset (WBD): Chapter 3 of Section A, Federal Standards, Book 11, Collection and Delineation of Spatial Data* (Vol. 11-A3, p. 54). Reston, VA: U.S. Geological Survey. https://doi.org/10.3133/tm11a3